NAVAL FACILITIES ENGINEERING SERVICE CENTER
Port Hueneme, California 93043-4370

TECHNICAL MEMORANDUM
TM-2335-SHR

GRAZING-ANGLE FOURIER TRANSFORM INFRARED SPECTROSCOPY FOR ONLINE SURFACE CLEANLINESS VERIFICATION

YEAR 1

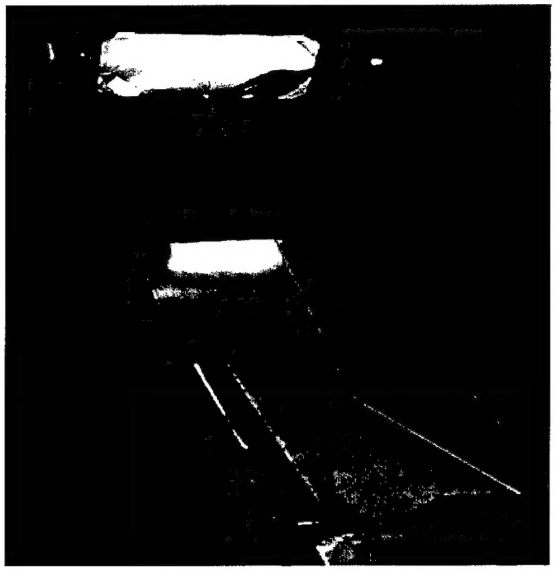

by

Theresa A. Hoffard
Calvin A. Kodres
Daniel R. Polly

July 2000

EXECUTIVE SUMMARY

As part of the Online Surface Cleanliness Project, the Naval Facilities Engineering Service Center (NFESC) conducted a study of grazing-angle reflectance Fourier Transform Infrared (FTIR) Spectroscopy as a tool for online cleanliness verification at Department of Defense (DOD) cleaning facilities. Examples of applications where surface cleanliness is critical include coating, plating, and bonding of aircraft parts; bearing refurbishment; and shipboard surface mounting of absorbing tiles. In cases such as these, visual inspection is often inadequate to detect contamination that will cause subsequent bonding or fouling problems.

NFESC partnered with Sandia National Laboratories, Livermore, California, under the sponsorship of the Strategic Environmental Research and Development Program (SERDP) in the development of two prototype instruments with complementary capabilities for cleaning verification. While Sandia conducted studies on an infrared laser imaging device, NFESC led the effort to develop grazing-angle reflectance FTIR technology into a real-time, on-site device for post-cleaning determination of surface contamination. In the project's first year, the feasibility of grazing-angle reflectance FTIR was demonstrated in the laboratory for the detection of organic contaminant residues on reflective surfaces. Substrates and residues chosen for the study are common to DOD components used in a variety of military and contractor assembly, fabrication, and repair facilities.

Results of the study revealed that grazing-angle reflectance FTIR is a very sensitive method for detection of organic residues on metallic surfaces, capable of detecting contaminants to $<1.0\ \mu g/cm^2$ with average baseline noise levels of ≤ 0.0001 reflectance-absorption units on flat surfaces. An evaluation of possible water interference from cleaning operations revealed that the presence of water up to approximately 5 μm (micrometers) in thickness did not diminish the quality of the FTIR spectral data. An evaluation of FTIR on curved aluminum samples was also conducted and revealed that a radius of curvature ≥ 1 cm results in a noise level average of $<$ 0.0004 reflectance-absorption units (factor of 4 times greater than flat surfaces of like-material) but still allows readable spectral data for ≥ 0.1 μm films.

Based on the results presented herein for Year 1, tasks for Year 2 of the project will include continuation of measurements on calibrated contaminants, designing and constructing the portable grazing-angle reflectance device, and collecting and analyzing DOD hardware samples on both the laboratory and portable devices. Year 3, the last year of the project, will be used to incorporate improvements to the portable device, build contaminant libraries into the device's software program, and field-demonstrate the device at selected DOD sites.

TABLE OF CONTENTS

1. INTRODUCTION

As part of the Online Surface Cleanliness Project, the Naval Facilities Engineering Service Center (NFESC) conducted a study of grazing-angle reflectance Fourier Transform Infrared (FTIR) Spectroscopy as a tool for online cleanliness verification at Department of Defense (DOD) cleaning facilities.

NFESC partnered with Sandia National Laboratories, Livermore, California, under the sponsorship of the Strategic Environmental Research and Development Program (SERDP) in the development of two prototype instruments with complementary capabilities for cleaning verification. While Sandia conducted studies on an infrared laser imaging device, NFESC led the effort to develop grazing-angle reflectance FTIR technology into a real-time, on-site device for post-cleaning determination of surface contamination. In the project's first year, the feasibility of grazing-angle reflectance FTIR was demonstrated in the laboratory for the detection of organic contaminant residues on reflective surfaces.

Applications where surface cleanliness is critical include coating, plating, and bonding of aircraft parts; bearing refurbishment; and shipboard surface mounting of absorbing tiles. In these cases, visual inspection is often inadequate to detect contamination that will cause subsequent bonding or fouling problems if not removed.

The information obtained through this laboratory study is being used in Year 2 of the project to design and build a portable real-time prototype device. This device will allow process operators to analyze parts on site and make determinations of subsequent cleaning actions, as well as aid in distinguishing between specific contaminants.

2. BACKGROUND

The instrumental detection and identification of organic contaminants on reflective surfaces is conveniently and rapidly done by FTIR reflective methods. However, while FTIR is a mature analytical technique, commercially available instrument configurations are not well suited for real-time analysis of low levels of surface contaminants (<< 1.0 micrometer). Current portable infrared devices are limited in sensitivity to surface contaminants by the nature of their optical designs.

FTIR sampling techniques such as attenuated total reflectance (ATR) and diffuse reflectance infrared transmission spectroscopy (DRIFTS) have been commercialized into compact hand-held designs. In these devices, infrared radiation contacts the surface to be analyzed at angles of incidence of near-normal to 60 degrees from normal, resulting in limited sensitivity to very thin layers of surface species.

"Grazing-angle" sampling technology, on the other hand, has been shown to maximize the sensitivity of infrared reflectance measurements for thin layers of organic materials on metallic surfaces. As early as the late 1950's, researchers have studied grazing-angle reflectance infrared spectroscopy (Refs. 1 and 2). Laboratory sampling devices employing grazing-angle reflectance technology are now commercially available. However, the technology has not yet advanced to the commercialization of a portable, on-site, and real-time device.

Grazing-angle reflectance theory can be explained by referring to Figure 1. In reflection spectroscopy, a portion of the incident radiation beam (in this case infrared) reflects off the surface of the thin film, while the remaining portion travels (is refracted) through the film and reflects off the substrate back through the film. This is known as "double-pass" reflection-absorption (Refs. 3 and 4)

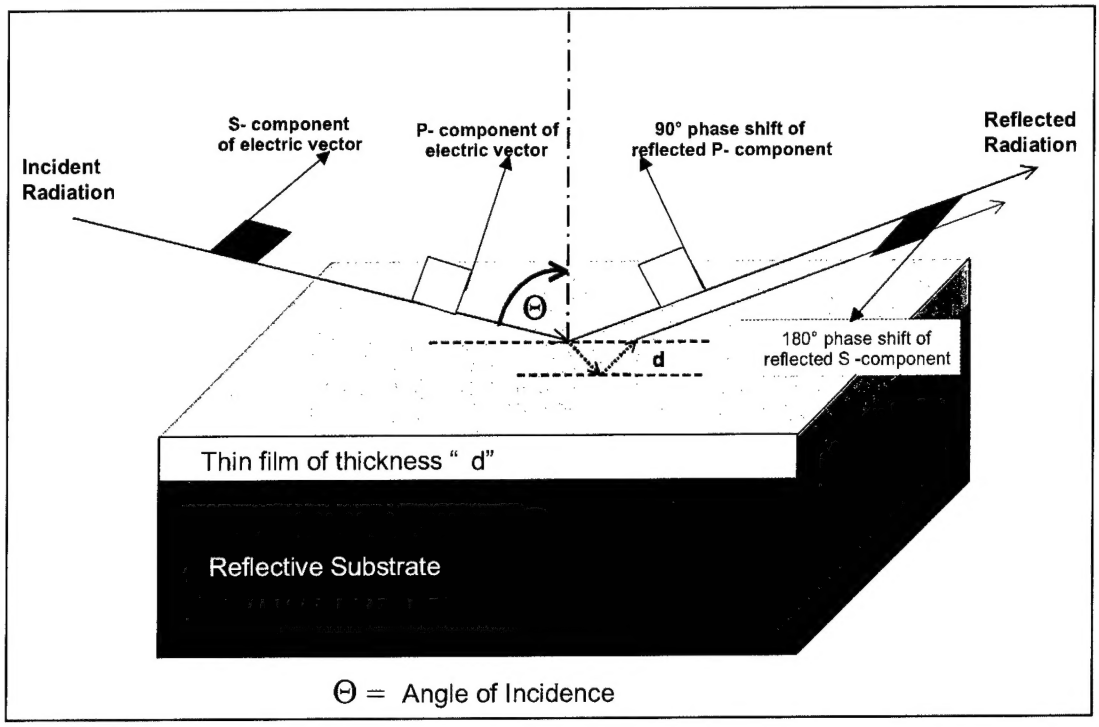

Figure 1. Infrared energy striking a contaminated reflective substrate at a grazing angle of incidence.

Predominantly, improved sensitivity at grazing angles results from the polarization phenomenon of electromagnetic radiation (Refs. 5 and 6). The electric vector of all electromagnetic radiation contains two components – the p-component and s-component. For radiation contacting reflective surfaces, the s-component, perpendicular to the plane of reflection (parallel to the plane of the surface), undergoes a phase shift of approximately 180 degrees. The vector sum of the incident and reflected s-component is almost zero at the surface; thus, the two cancel each other out. At grazing angles, the p-polarized component undergoes a phase shift at the surface from approximately 20 to 180 degrees, depending on the exact angle of incidence. At large incident angles, this phase shift is approximately 90 degrees (Ref. 6). The vector sum of the incident and reflected p-component now give an intense electric field oriented perpendicular to the reflecting surface. When passed through a polarizing lens, the s-component of the reflected radiation can be filtered out and only the p-component is detected and converted to a spectrum.

Additionally, at large angles of incidence, the infrared beam contacts the contaminant–laden surface at an increased effective path length through the infrared-

absorbing material. In accordance with Beer's Law of absorbance, this enhances the absorption, which results in a stronger FTIR "signal" of the contaminant (Ref. 7).

FTIR uses infrared radiation to characterize and quantify organic (and many inorganic) materials. At the molecular level, an organic substance absorbs infrared energy and undergoes vibrations at discrete frequencies, or wavelengths, according to its unique chemical makeup. A graph of the energy absorbed versus the infrared frequency in wavenumbers (inversely proportional to wavelength) is called the "spectrum" of that material. Unique chemical functional groups produce distinct absorption patterns. For a pure compound, the spectrum becomes a fingerprint of identification. For unknown materials or mixtures such as paints, a spectrum may classify the material as being from a particular chemical family(e.g., a urethane or epoxy). However, it may not always provide enough information to identify the pure components.

Figure 2 shows a typical reflectance-absorbance FTIR spectrum. The "peaks" or "bands" represent infrared light absorbed by the chemical species being analyzed. The two spectra represent a very thin film of electrically-insulating grease on an aluminum substrate analyzed at 30 and 75 degrees (grazing-angle), respectively. The absorbance of the infrared energy in the material is dramatically enhanced at 75 degrees. In the enhanced spectrum, the location and shape of the peaks allow an FTIR analyst to classify this material as a silicone.

3. EXPERIMENTAL PROCEDURES

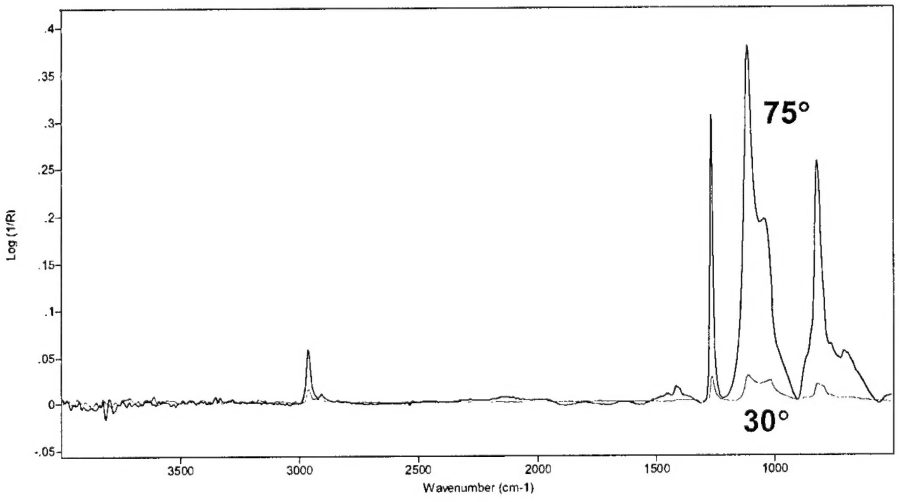

Figure 2. Comparison of a 0.2 μm silicone film on aluminum analyzed at 30°and 75°.

NFESC conducted a series of laboratory experiments to meet the Year 1 milestones of the project. Instrumental analysis was performed on NFESC's Biorad FTS-60 research-grade FTIR, unless otherwise stated. A standard DTGS room-temperature detector was utilized and approximately 260 scans were taken for each spectrum. Corresponding background spectra were collected using clean metal substrates at several angles, roughness values, and orientations of interest.

Background spectra are used to ratio sample "single beam" scans and convert them to reflectance-absorption spectra.

3.1. Construct Optical Interface – Laboratory Version

Constructing the optical interface was readily accomplished because of the availability of commercial grazing-angle reflectance sampling devices for laboratory FTIR. A grazing-angle sampling device was procured from a commercial FTIR accessories vendor and installed into NFESC's research-grade laboratory FTIR instrument (see Figure 3). This interface was a variable-angle device, allowing analysis of a variety of reflective parts at incident radiation angles of 30 to 80 degrees.

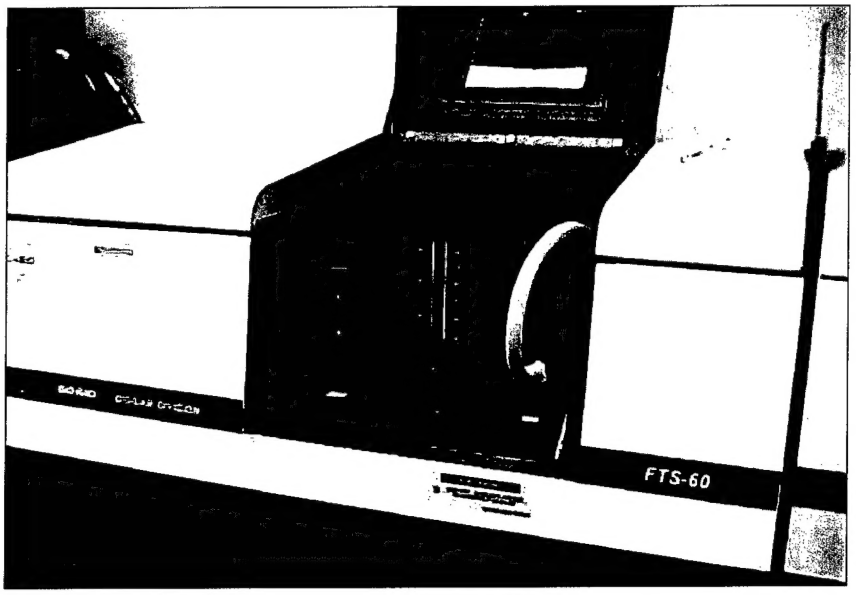

Figure 3. FTIR with variable-angle optical interface.

A critical Go/No-Go milestone for Year 1 of the project was to demonstrate the experimental noise level as a signal-to-noise ratio for flat reflective substrates. Low noise levels in the spectra allow weak absorption peaks of very thin films to be seen above the baseline. A goal of <0.0001 reflection-absorption units noise was set for the laboratory interface device. A 600-grit aluminum panel contaminated with approximately 0.08 μm organic residue was used for the measurements. Two spectral frequency regions free from interference due to absorbing species were examined. The spectral baselines were fit with third-order polynomials by Sandia National Laboratories' specialized software and the differences plotted versus baseline. Calculated standard deviations of the differential curves were taken as the average noise levels.

3.2. Evaluate Sensitivity to a Generic Hydrocarbon Contaminant

Evaluation of grazing-angle reflectance sensitivity to hydrocarbon contaminants was accomplished by analysis of vapor degreased aluminum panels with simulated shop grease contamination. These panels were obtained from a previous NFESC project, "Surface Quality Impact of Replacing Vapor Degreasers with Aqueous Immersion Systems" (Ref. 8). During this project, aluminum panels were purposely soiled with a mixture of typical shop lubricating compounds, then cleaned using either a vapor-degreasing method (using trichloroethylene) or an aqueous biodegradable cleaner. The results of the project revealed that the aqueous cleaner was superior to the organic solvent in cleaning the shop soils from aluminum. The panels were analyzed before and after cleaning using DRIFTS-FTIR (a diffuse reflectance sampling method).

During the current SERDP project, selected vapor-degreased panels were analyzed by the grazing-angle method. A variety of instrument parameters including angle of incidence, masking, polarization, and aperture setting were altered to evaluate changes in the quality of the spectra.

3.3. Demonstrate Contaminant Detection Method

3.3.1. Prepare calibrated test samples

Appendix A lists the samples prepared during Year 1. The selected metal substrates were chosen based on usage data obtained from military and contractor facilities. Likewise the selected candidate contaminants are materials actually used at these facilities and known to be difficult to remove during cleaning operations. Table 1 shows the suite of contaminants utilized for the Year 1 effort.

Table 1. Year 1 Candidate Contaminants

Material	Description	Usage
A	White soft solid – ester grease	Metal drawing, cutting, and lubricating agent
B	Brown liquid – paraffin hydrocarbons	Rust preventative, cleaner, lubricant, protectant for metals
C	Semi-transparent silicone grease	Electrical insulating compound

Six surface roughness finishes of the aluminum test coupons were obtained, ranging from 80 to 600 grit (600 grit being the smoothest). Grit refers to the sandpaper

finish used by the vendor to create the surface profiles. Two surface roughness levels, 600 and 220 grit, were obtained for the remaining metal types. A profilometer was used to examine the surface roughness profiles and provide "R_a" values (in micrometers or micro-inches). R_a roughness, the arithmetic average roughness, is a term used for machined surfaces. It is the arithmetic average of the absolute deviations from the mean surface level. Due to the nature of metal shop finishing processes, surface roughness values can vary considerably across a given surface area. The metal surfaces of the coupons, upon finishing at the vendor's facility, acquired a directional "grain" parallel to the coupons' longitudinal axis. Figure 4 shows the variation in surface roughness for the aluminum panels and the relationship to grit finishes.

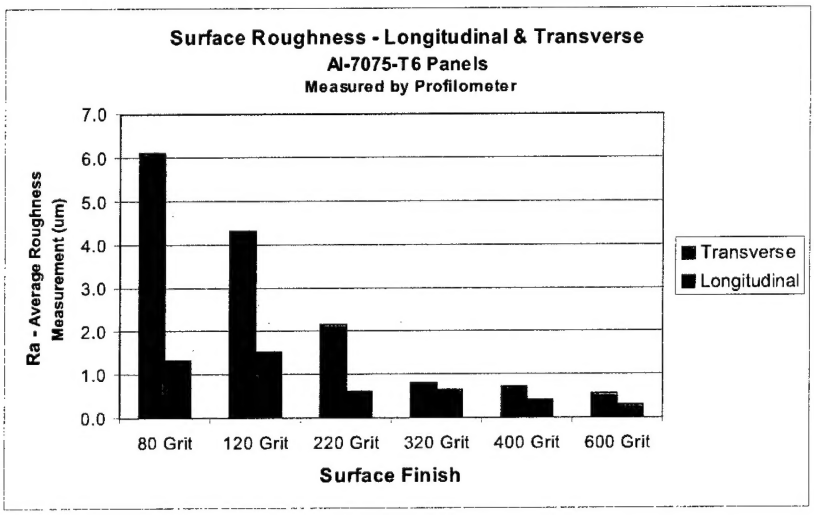

Figure 4. R_a values related to surface finish levels of the test panels.

Prior to contaminant application, the panels where washed with acetone, then cleaned by sonication with a clean-rinsing aqueous cleaner. They were thoroughly rinsed and either oven-dried at 50°C or allowed to air dry after blotting. Once cooled, they were weighed on a semi-microbalance to the nearest 0.01 mg. Two or more weighings over the course of two to three days were averaged. No evidence of rusting was seen on the surfaces of the steel C4340 panels that were dried promptly after cleaning.

Both contaminant A and B were applied by two deposition methods – airbrushing and manual brushing (see Figures 5 and 6). Several other techniques were attempted, including wire-cator drawing, coupon spinning, and drop and spread (the solution was allowed to flow while the substrate is tipped to each side). They were abandoned due to the superior results obtained from the airbrushing and manual brushing. Contaminant C was applied by manual brushing only.

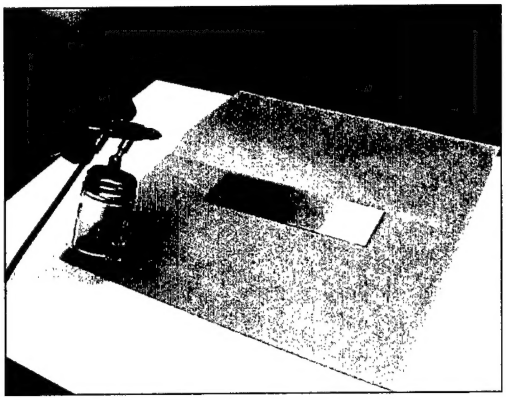

Figure 5. Contaminant being applied to an aluminum panel by airbrush.

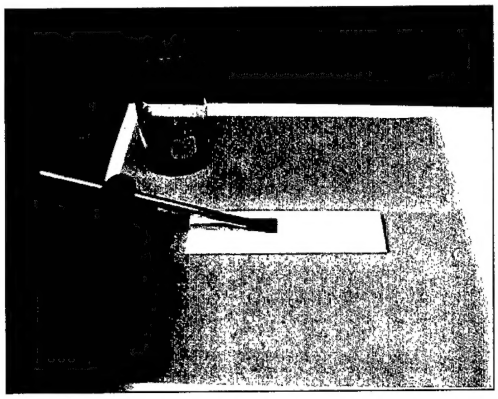

Figure 6. Contaminant being applied to an aluminum panel by manual brushing.

Contaminant A was mixed in a water solution for application, while contaminant B was applied as a solution in pentane. Contaminant C was initially dissolved in toluene to precipitate out the small amount of silica filler, then applied to the substrates in a toluene-pentane solution (the pentane allowing for better "wetting" of the substrate). Different film thickness levels were achieved by altering the contaminant-to-solvent ratios.

Contaminated samples were gently heated in a 50°C oven for 1 to 3 days to remove any semi-volatile and volatile components. This served to stabilize the contaminants, allowing for quantitation by weighting. Once the weights became stable, final weight averages were recorded. When not being analyzed, the samples were kept in a desiccator.

3.3.2. Demonstrate the grazing angle method on a variety of reflective surfaces using a selection of organic materials actually used in DOD shop environments.

Reflective surfaces analyzed for this task consisted of Aluminum 7075-T6, Stainless Steel 304, Steel Alloy C4340, and Titanium 4Al-6V (see Appendix A and Figures 7 and 8). The organic contaminants are described in Table 1.

Test coupons were analyzed with NFESC's laboratory FTIR and grazing-angle reflectance sampling device. Samples containing contaminant A were analyzed at 75 and 80 degrees. Upon preliminary review of the spectral output, it was determined that setting this particular sampling device to 80 degrees was increasing baseline noise without significantly enhancing the peak intensities in proportion to the noise. Thus 80-degree measurements were not taken for subsequent sample sets. The smoothest samples for contaminants B and C were analyzed at 60 degrees, as well as 75 degrees.

Theoretically, incident angles of 80 to 85 degrees provide the greatest enhancement of the reflectance-absorption signal for metal substrates. However, the

configuration of a particular instrument and sampling device optics, as well as the characteristics of the sample may dictate using a smaller angle.

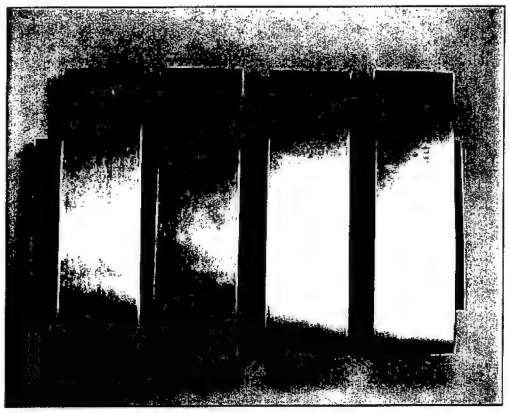

Figure 7. Aluminum, Titanium, Stainless Steel, and Steel Alloy (from left to right).

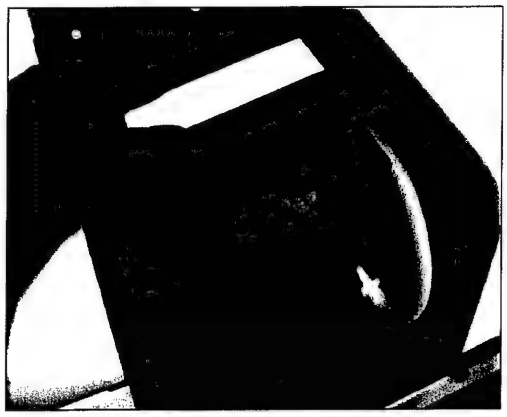

Figure 8. Coupon being placed longitudinally onto sampling device.

3.3.3. Demonstrate effects of surface roughness on the spectral output for a given reflective substrate.

Appendix A shows the variety of surface roughness values for the analyzed samples. Values were selected as a result of feedback from potential FTIR users at DOD and contractor fabrication and repair facilities. Due to the oriented nature of the roughness patterns, the samples were placed into the sampling device in both longitudinal and transverse directions. Thus, two spectra were generated for each sample (Figure 9).

In addition to the smoothest coupons, for contaminants B and C, a selection of rougher test coupons were analyzed at 60 degrees as well as 75 degrees (all coupons were analyzed at 75 degrees).

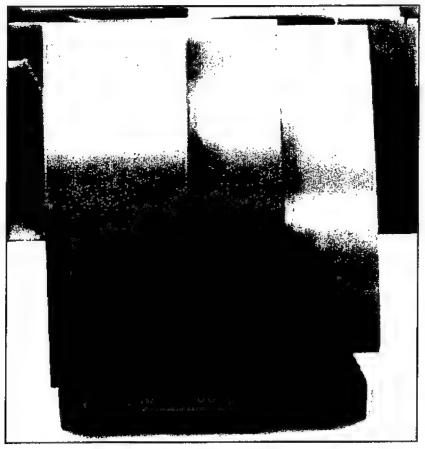

Figure 9. Surface roughness values 600, 320, and 80 grit (from left to right).

3.3.4. Demonstrate effects of residual surface water on the spectral output for a given substrate.

Test coupon number 419, containing approximately 0.22 μm of contaminant B, was chosen to conduct the residual water interference experiments. Contaminant B is insoluble in water and therefore not affected by repeated applications of water onto the coupon surface (by a non-contacting airbrush).

After each application of water, the coupon was immediately weighed and the weight loss tracked and recorded over time for up to 4 minutes. This allowed for a rough estimate of the amount of water remaining on the coupon's surface when the coupon was removed from the balance and placed in the FTIR for immediate analysis.

Between application and analysis cycles, the coupon was allowed to dry and retested to ensure that the spectral pattern of the contaminant had not degraded from that of the original scan before water application.

3.3.5. Demonstrate the ability of the method to provide readable spectra for non-flat reflective samples (≥ 1-cm radius of curvature).

A suite of six aluminum cylinders was prepared using aluminum foil and cylindrical sample bottles with a 1-cm radius of curvature. Pieces of the aluminum foil were cut to the same size as the rectangular sample coupons. The pieces were weighed before and after application of contaminant-B onto the "dull" side (by manual brushing). The foil samples were allowed to dry in a 50°C oven before final weighing. The foil pieces were then wrapped around the cylindrical bottles to create the samples. Each cylinder was analyzed in the longitudinal (Figure 10) and transverse orientation in relation to the infrared beam. All were run at 75 and 60 degrees for both orientations.

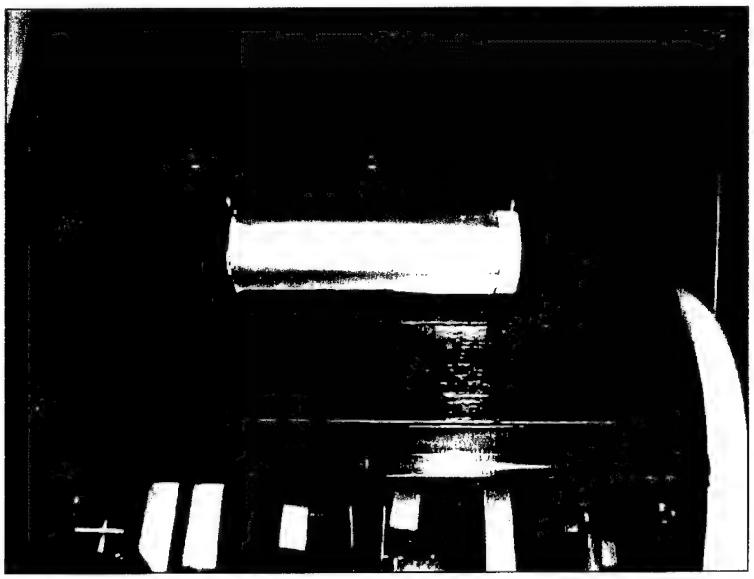

Figure 10. Cylinder being analyzed in a longitudinal orientation.

4. RESULTS

4.1 Generic Hydrocarbon Sensitivity

Aluminum panels soiled with a mixture of shop lubricants, baked on, then vapor degreased in trichloroethylene (TCE), were analyzed on the grazing-angle reflectance device. The vapor degreasing method was able to remove over 90 percent of the lubricant residue. However, thin films still remained on the surface (Ref. 8). The original films were several micrometers thick. Sandia National Laboratories, in their cooperative laser research, were able to estimate the remaining thin film on a representative panel at approximately 0.014 μm (Ref. 9).

The grazing-angle reflectance spectra were compared to spectra of the same panels obtained by diffuse reflectance FTIR. Figure 11 shows the difference in peak intensities between two spectra of the same panel. Peaks in the diffuse reflectance spectrum are barely visible in comparison to the same peaks in the grazing-angle reflectance spectrum (75-degree angle). For the FTIR analyst, accurate interpretation of peaks and classification of the film as a long-chain aliphatic hydrocarbon is definitive with the grazing angle spectrum. In contrast, the peaks in the diffuse reflectance spectrum are not appreciably above the level of the baseline noise, especially at the lower wavenumbers, making it infeasible to accurately classify the surface contaminant.

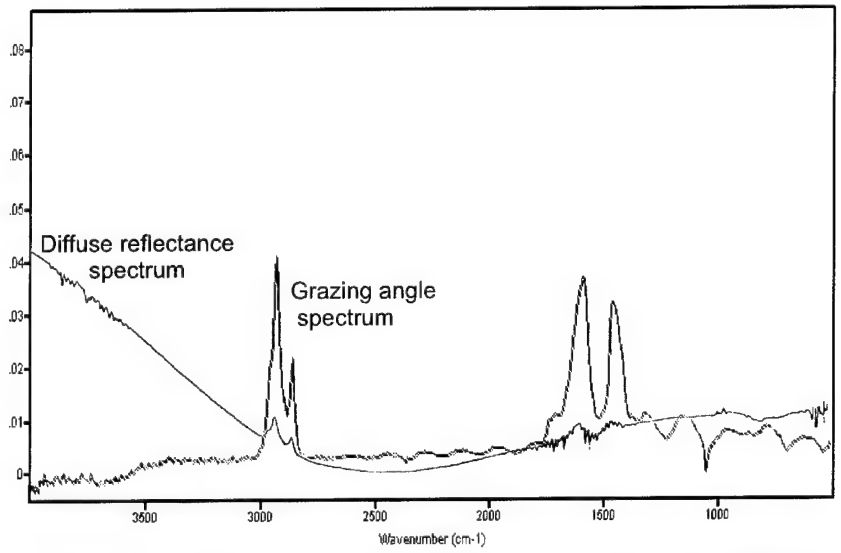

Figure 11. FTIR spectra of vapor-degreased panel by diffuse reflectance and grazing-angle reflectance.

Instrumental parameters of the optical interface and FTIR were altered to examine their effect on the grazing-angle reflectance spectra. Figure 12 shows the spectral enhancement of the C-H stretching peaks for a vapor-degreased panel as the incident angle on the optical interface is increased to a grazing-angle.

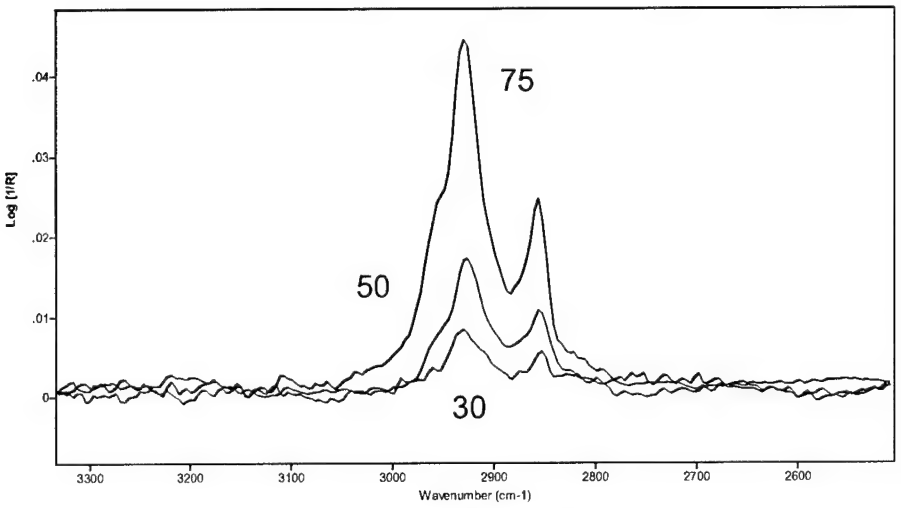

Figure 12. Spectra of a vapor degreased aluminum panel at varying angles of incidence.

Figure 13 shows the C-H stretching spectral region of a vapor-degreased panel analyzed at 75 degrees with s-polarization, no polarization, and p-polarization of the reflected radiation, respectively. The spectral peaks are enhanced significantly with p-polarization.

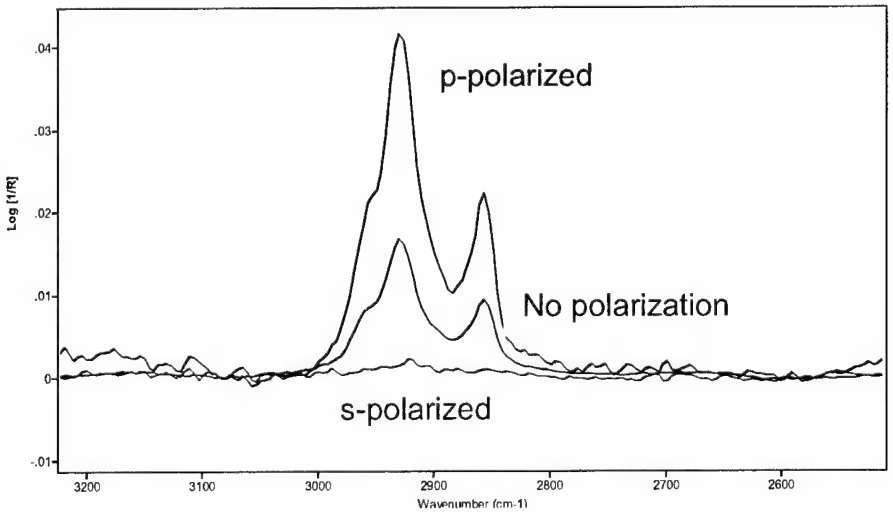

Figure 13. Spectra of a vapor degreased panel showing the effects of polarization.

The particular configuration of the laboratory optical interface allows for the analysis of parts from approximately 10 mm in diameter (round or flat) to infinitely large (as long as the part contains analyzable sections at no greater than 1-cm in curvature or no less than approximately 10 mm diameter). At 75 degrees, incident infrared

radiation is focused on the sample's surface as an ellipse, 10- to 12-mm in width (Ref. 10). A non-absorbing "mask" can be placed over the device's sampling opening to allow alignment of a small sample surface area with the focused beam location.

The effects of using a mask on flat reflective surfaces were examined using the vapor-degreased panels. Without a mask inserted onto the optical interface, almost the entire surface of the panel (3.8 by 12.7 cm) is exposed to the chamber of the device, allowing radiation outside the 10- to 12-mm beam width to also strike the panel and reflect back to the collection optics. With the mask in place, radiation outside the 10- to 12-mm window does not reflect off of the panel. Some light may reflect off of the mask and be captured as scattered light, but its contribution to the intensity of the sample absorption is not significant.

Figure 14 shows a comparison of a panel analyzed with and without a 1.27-cm mask. Installing the mask results in a slight decrease in C-H-stretching peak intensity, as well as an increase in baseline noise. However, the differences are insignificant in relation to the overall intensity of the reflectance-absorbance, indicating that using a mask to align the sample surface to the beam does not significantly impair the spectrum.

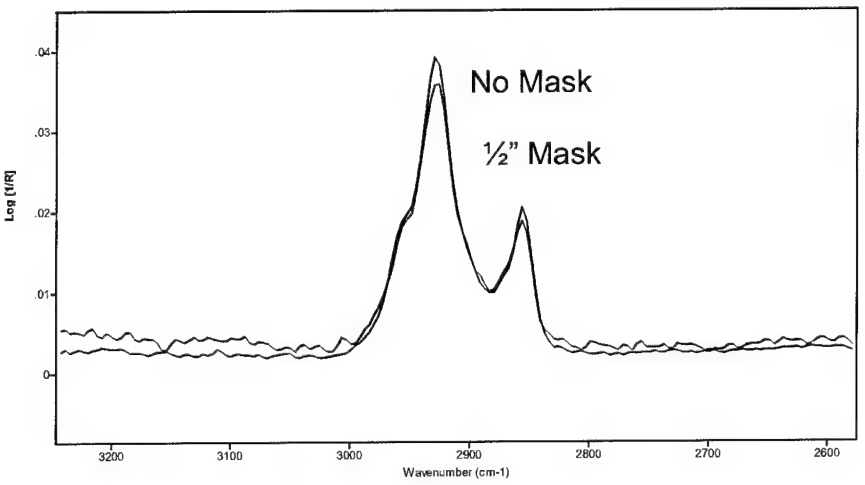

Figure 14. Spectra of a vapor degreased panel showing the effects of masking.

Another parameter of the FTIR measurement is aperture setting. The aperture is a device inside the FTIR that limits the amount of infrared light reaching the sample compartment. This is important at high resolution spectral settings where it is required to minimize a phenomenon known as "angular divergence" (Ref. 3.).

The infrared beam inside the instrument is not perfectly cylindrical in shape, but rather conical. This causes the outer light rays to be at an angle to each other and destructively interfere with each other. Using an aperture prevents some of this diverging light from reaching the sample, but it also results in a loss of signal to the detector.

Angular divergence must be decreased for higher resolution settings. The resolution of the FTIR refers to its ability to distinguish spectral features that are close

together in a spectrum. Higher resolution settings, however, result in increased spectral noise and are usually only used for analyzing gaseous samples. At a medium resolution setting of 8 cm^{-1}, used for all of the analyses in this study, the aperture setting did not significantly improve the quality of the spectra. Figure 15 shows a vapor degreased panel scanned at both an open aperture and a 2-cm^{-1} setting. Changing the FTIR's aperture setting had little effect on the spectrum.

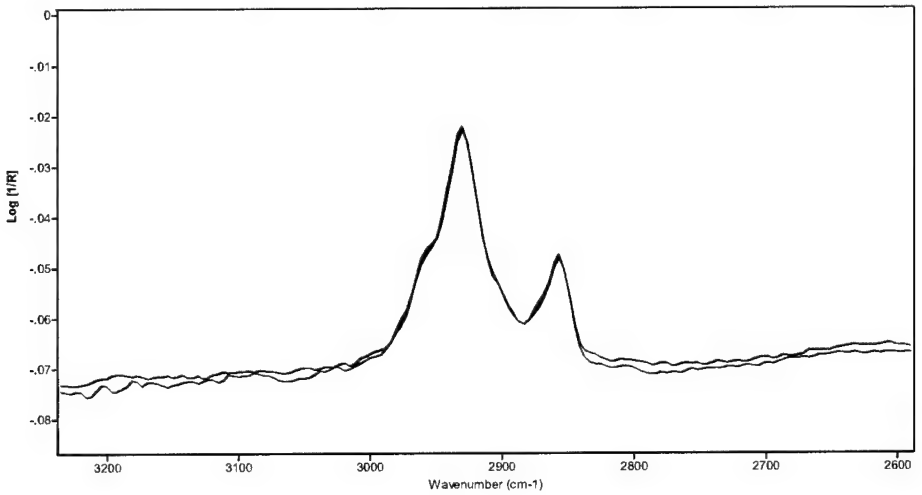

Figure 15. Spectra of a vapor degreased panel showing the effects of aperture setting.

4.1.1 Noise levels of flat reflective substrates

The goal of a reflection-absorption noise level <0.0001 was successfully met (Ref. 7). Figure 16 presents the results. The resultant average noise levels are 0.3 x 10^{-4} and 1.0 x 10^{-4} for the two spectral regions. A noise level of 1 x 10^{-4} was used for an estimate of hydrocarbon detection limits at frequencies near 2,900 cm^{-1}. Using the Environmental Protection Agency's (EPA) Lower Limit of Detection (LLD) formula results in a log [1/R] value of 0.00046 corresponding to a minimum detectable film thickness of 0.0036 μm (or an area concentration of 0.34 $\mu g/cm^2$).

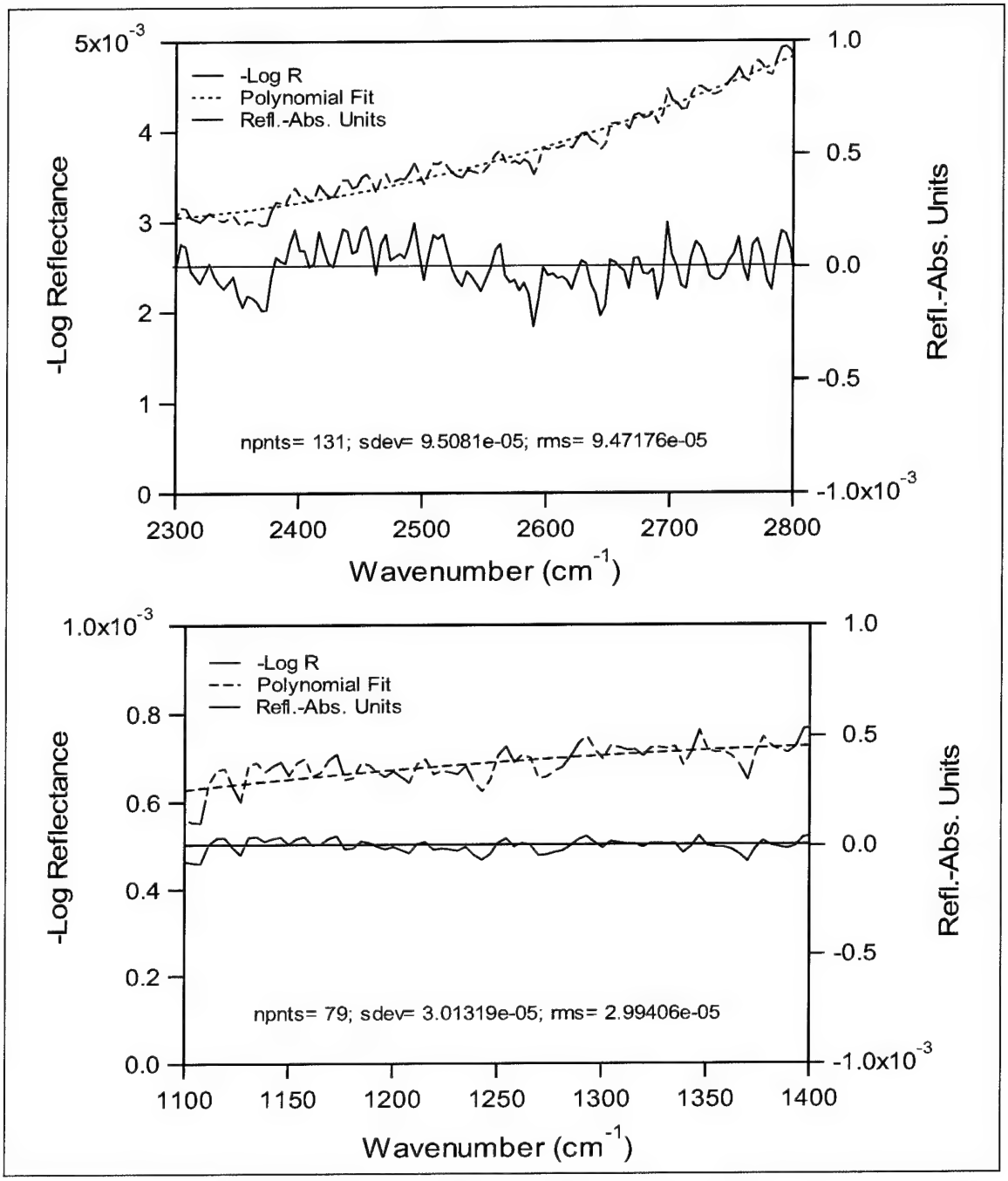

Figure 16. Experimental data for a 600-grit aluminum panel fit by third-order polynomials. Standard deviations = average noise levels.

4.2 Grazing-Angle Method Demonstration

4.2.1 Sample Preparation

The uniformity of the films applied to the substrate test samples varied with physical properties of the contaminants. Both contaminant A and C were difficult to apply on the sample surfaces; both materials are semi-solid greases. Contaminant B is a liquid already contained in a hydrocarbon solvent. Diluting the material with pentane resulted in homogeneous solutions that were easily applied onto the substrates.

Contaminant A is not soluble in any common solvent. It is partially miscible in water, however, forming a milky suspension with undissolved fine particles. Application of this suspension resulted in slight to moderate "streaking" of the contaminant on the surfaces of the substrates, indicating lack of uniformity in the film thickness. Melting the grease onto the substrates was not feasible due to its high melting point.

Contaminant C was found to be relatively soluble in toluene (with the exception of a 5- to 20-percent silica component that drops out of solution if left undisturbed for several hours). However, the toluene solution did not adequately "wet" the substrate surfaces. Upon application, the solution immediately beaded up, leaving only spot coverage of the contaminant after evaporation of the toluene. Contaminant C does not dissolve in pentane, but it was found that mixing pentane into the toluene solution immediately before application allowed the solution to wet the entire substrate surface. Upon evaporation of both toluene and pentane, some film streaking was visible but less severe than the contaminant A samples.

Sandia National Laboratories' complementary detection device was able to map the relative contaminant coverage on the samples (Ref. 7). Figure 17 is an example of this mapping and demonstrates lack of film thickness uniformity of the contaminant A samples. The red areas reflect the thickest regions of the film, the blue reflects the thinnest regions.

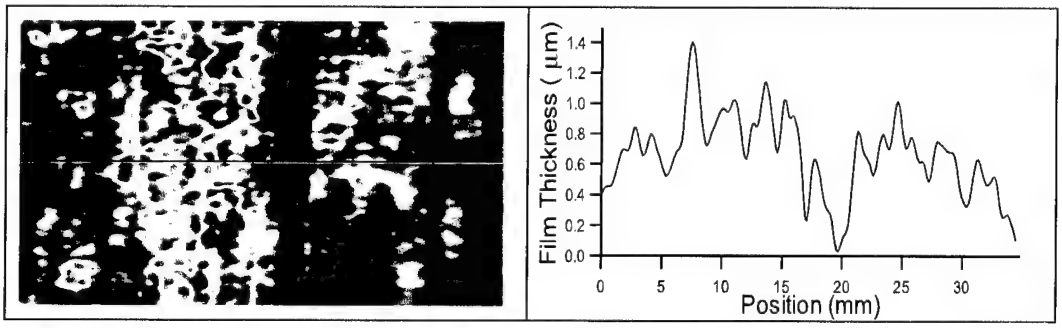

Figure 17. Infrared-laser image and corresponding line film-thickness plot for Contaminant A on an aluminum panel.

4.2.2. Variety of reflective surfaces

Optical properties of a substrate affect reflectance spectra since the infrared beam reflects off the substrate, as well as being absorbed by the thin film. Two properties, the "absorption index" and the refractive index, are of primary consideration (Ref. 6). The greater these values, the more reflective the material. Highly reflective materials allow more incident radiation to be reflected and detected in the FTIR. Metals are significantly more reflective than non–metals and their conductive nature allows for enhancement of the p-component of the infrared radiation.

During the first year of the SERDP project, selected metals listed in Appendix A were examined for their ability to reflect infrared radiation and provide readable spectra when coated with thin films of the selected contaminants. Background spectra were collected for the bare metals before contamination. Figure 18 shows the single beam background spectra of 600 grit substrates, (which look significantly different than the final sample spectra). The Y-axis indicates relative intensities of infrared radiation reaching the FTIR detector (i.e., the relative reflectivity of the metals). From Figure 18, it is evident that the aluminum-7075 is the most infrared-reflective metal of the four, under the specified conditions.

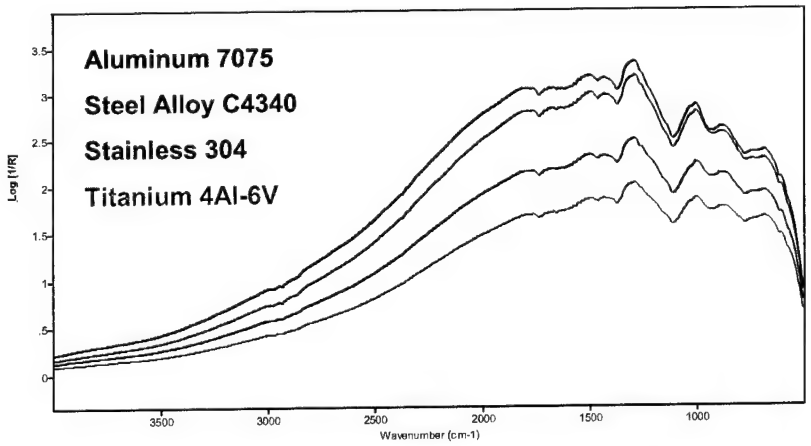

Figure 18. Single beam background spectra of four metal substrates. All coupons were 600 grit, scanned at 75° and longitudinal orientation.

Figure 19 is a comparison of contaminant C reflectance spectra on the four metal surfaces. The spectra exhibit reflectance-absorbance values for a film of approximately 0.11 μm. The spectra were adjusted to compensate for the differing film thickness values, originally at 0.047, 0.112, 0.128, and 0.075 μm on aluminum, steel alloy, stainless, and titanium, respectively.

Analyzing contaminant C on aluminum expectedly results in the largest enhancement of the signal intensity, followed by the steel alloy, stainless steel, and lastly titanium. For these thin films, the readability of the spectra on all four substrates

is excellent – all peaks of the silicone in this spectral region are clearly defined with low baseline noise.

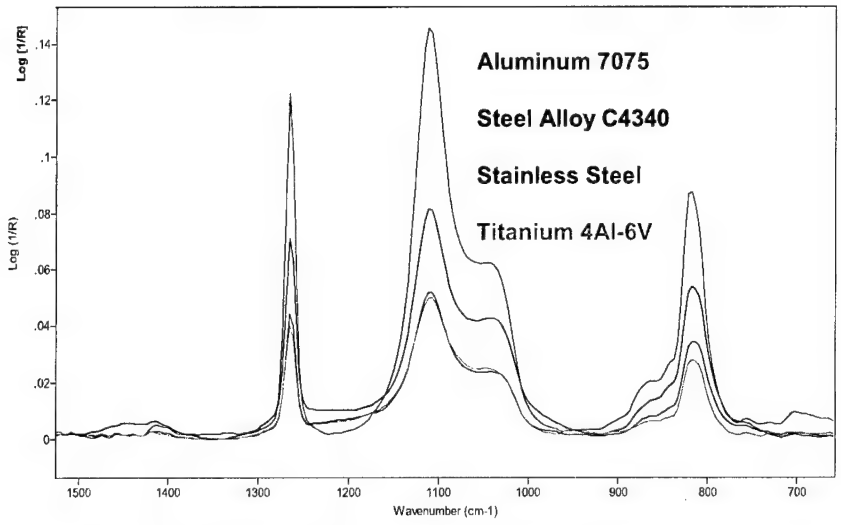

Figure 19. Silicone on several reflective surfaces. Spectra corrected to same film thickness value.

4.2.3. Surface roughness comparisons and effect of contaminant optical properties

Surface roughness is another important factor affecting a reflectance spectrum. The degree of scatter of incident radiation is greater with rough surfaces, resulting in less energy arriving at the detector (Ref. 6). This scattering increases further at grazing angles of incidence.

Figures 20 through 25 show the qualitative degradation of the spectra when going from a smooth reflective surface (600 grit) to a relatively rough surface for similar amounts of contaminant. The loss of quality is manifested as an increase in baseline noise (especially at higher wavenumbers), a decrease in baseline linearity, and sometimes by sinusoidal "fringe" patterns appearing in the middle to upper portions of the spectra.

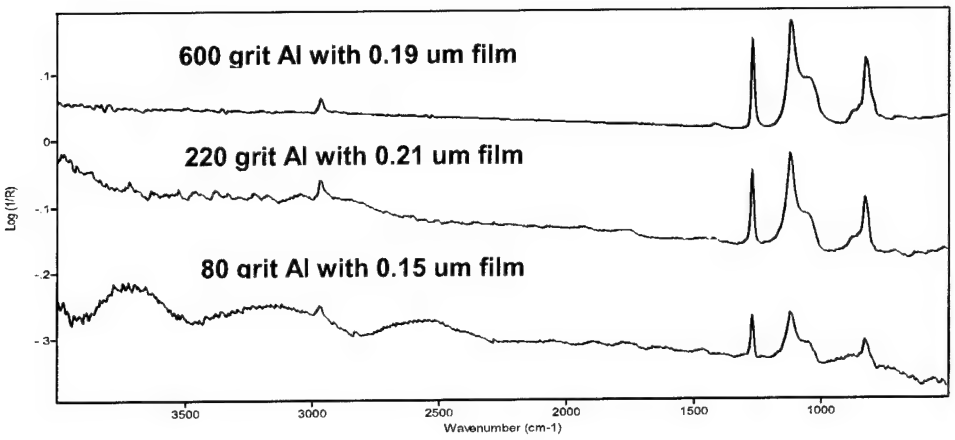

Figure 20. Transverse data showing effects of increasing surface roughness for Contaminant C on aluminum.

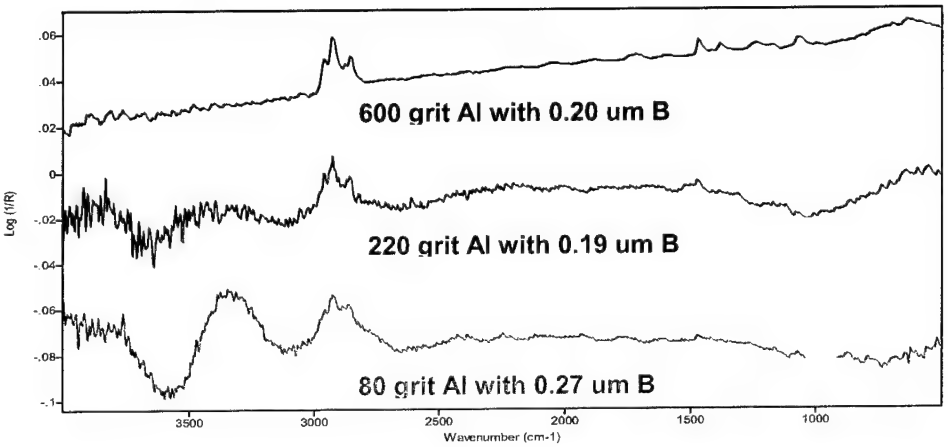

Figure 21. Transverse data showing effects of increasing surface roughness for Contaminant B on aluminum.

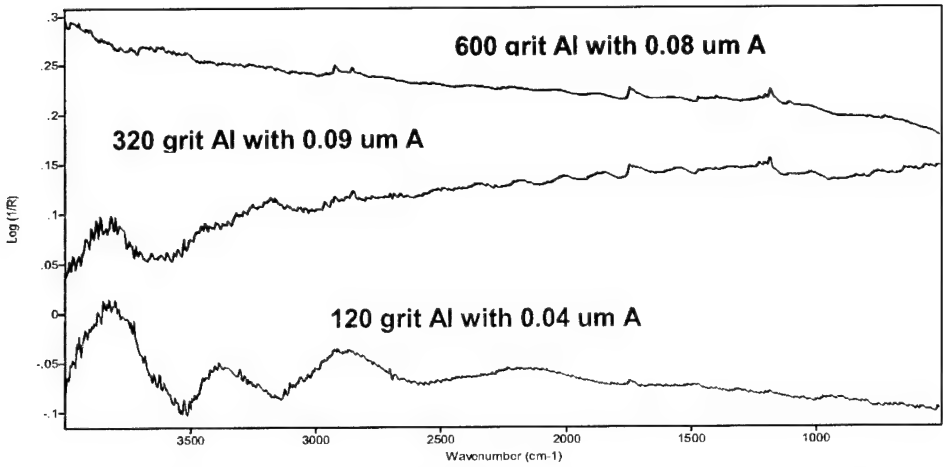

Figure 22. Transverse data showing effects of increasing surface roughness for Contaminant A on aluminum.

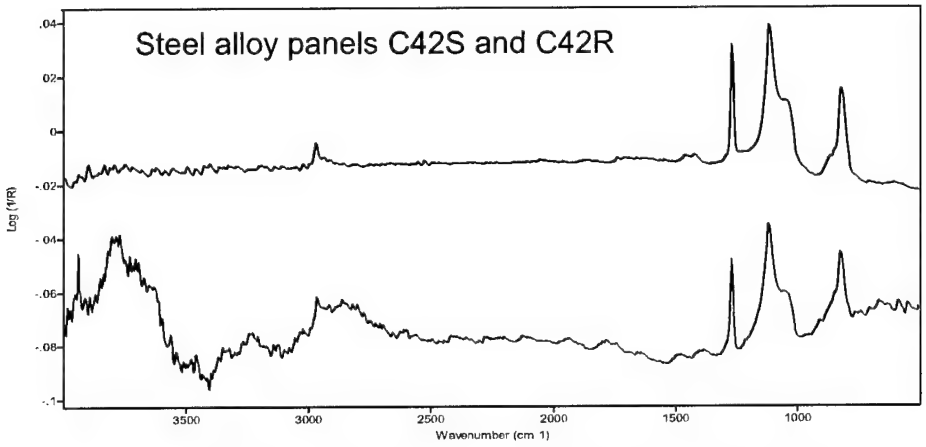

Figure 23. Transverse data showing effects of surface roughness for Contaminant C on steel alloy C4340.

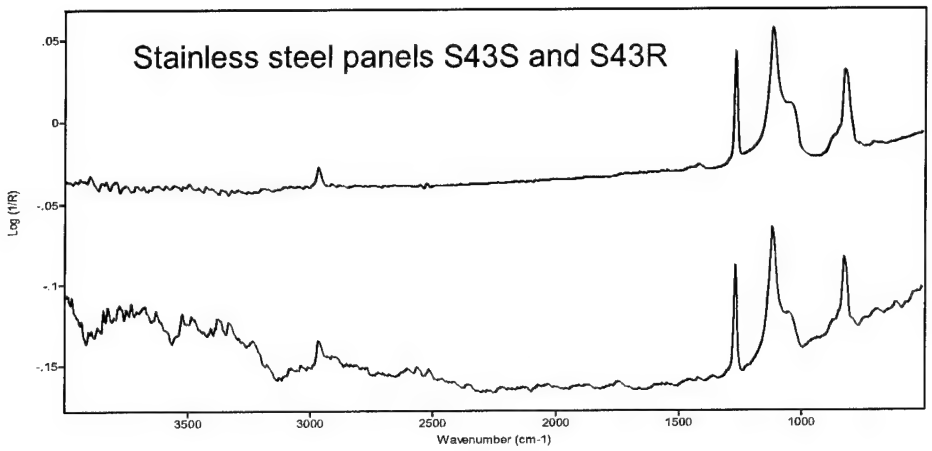

Figure 24. Transverse data showing effects of surface roughness for Contaminant C on stainless 304.

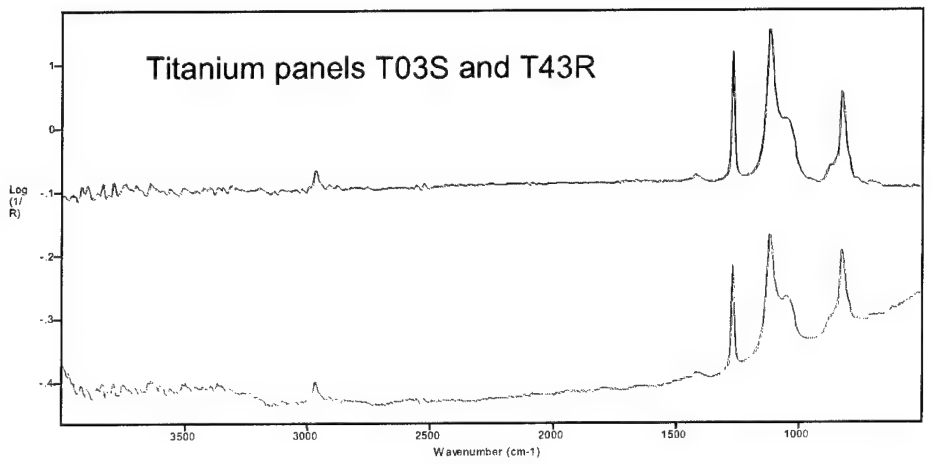

Figure 25. Transverse data showing effects of surface roughness for Contaminant C on titanium.

The test coupons (600 to 80 grit) were all run longitudinally and transversely on the FTIR optical device. The raw data were sent to Sandia National Laboratories for statistical processing. Hydrocarbon spectral peaks were fit by a least-squares analysis that allows for quantitative analysis and comparison of the contaminants. Output data are presented in Figures 26 and 27 for contaminants A and B on aluminum. The graph points represent film thickness on individual coupons versus the integrated peak intensity of the spectra. Reflectance-absorbance theory states that the intensity of spectral peaks is proportional to contaminant thickness, and ideally, is linear within a range of film thickness values.

Analysis of the reflectance-absorption data for contaminants A and B reveals lower integrated intensities for transverse measurements than for longitudinal

measurements (at a given film thickness). This is predictable and due to the larger surface roughness values encountered in the transverse orientation.

For contaminant A, there is a marked departure from linearity at the highest values of film thickness for coupons rougher than 600 grit. This may be attributable to the morphological characteristics of contaminant A. Contaminant A is a semi-solid grease that forms slightly opaque films at higher thickness values. Additionally, contaminant A's lack of solubility may have resulted in accretion of solid particles along the grooves and ridges of the surface. At a 75-degree angle, this could result in shadowing of the infrared beam by the contaminant.

In contrast, the graphs for contaminant B reveal relatively good linearity for both longitudinal and transverse measurements. Again, the morphology of the material may explain this change. Contaminant B is a paraffin liquid, soluble in a number of organic solvents, and free-flowing. This allows an applied film to conform more closely to the surface topography of the test coupons, creating a "smoother" profile for the reflecting infrared beam.

Sandia National Laboratories also analyzed contaminant A at a lower angle of incidence, 60 degrees (Ref. 7). At this angle, the shadowing effect of the contaminant is reduced for all but the roughest samples. The longitudinal and transverse measurements (Figure 28) both exhibit improved linearity over that of the 75-degree measurements except for the 80 grit samples. However, the relative intensities of the selected peak are lower.

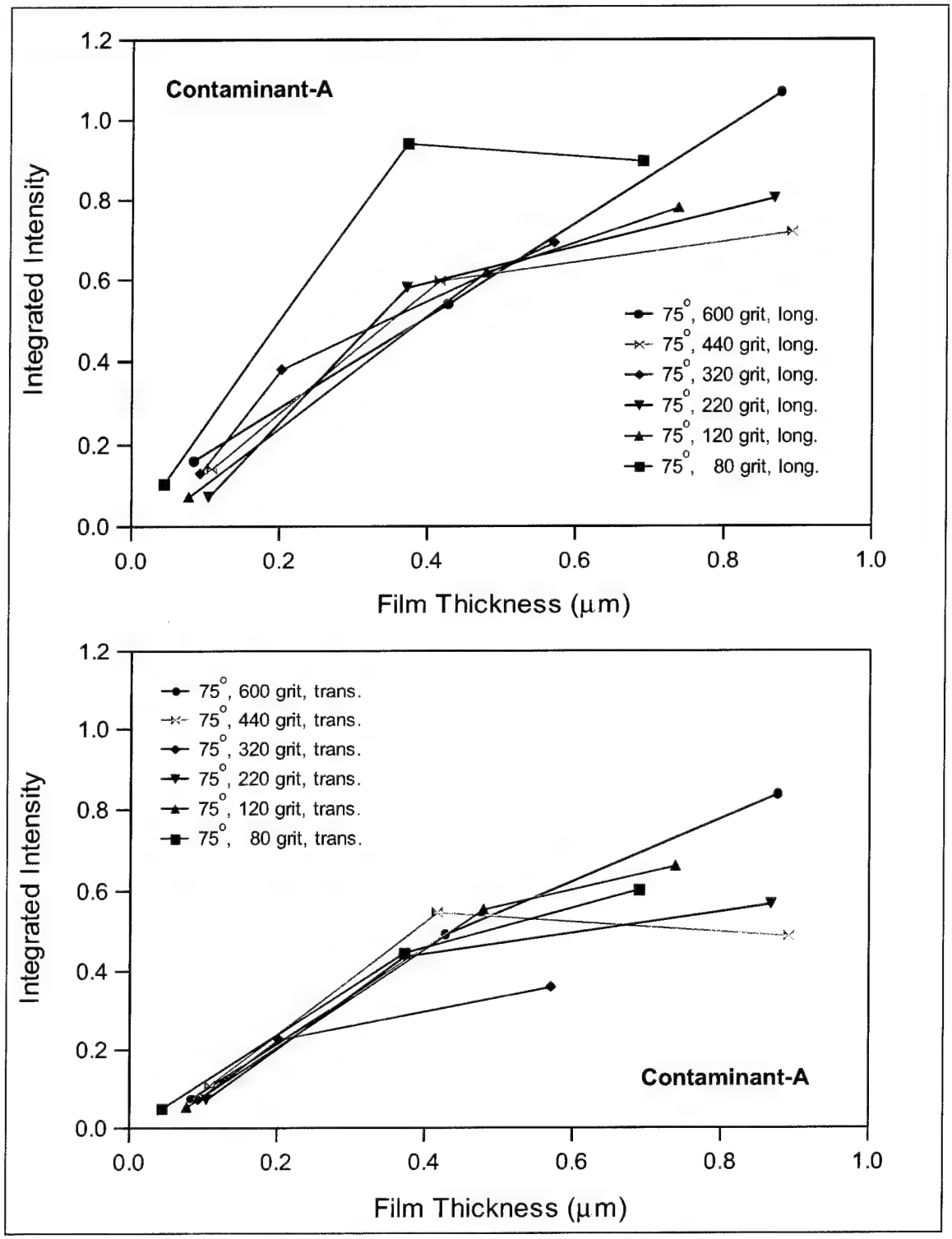

Figure 26. Integrated C-H peak intensity for spectrum of Contaminant A on aluminum.

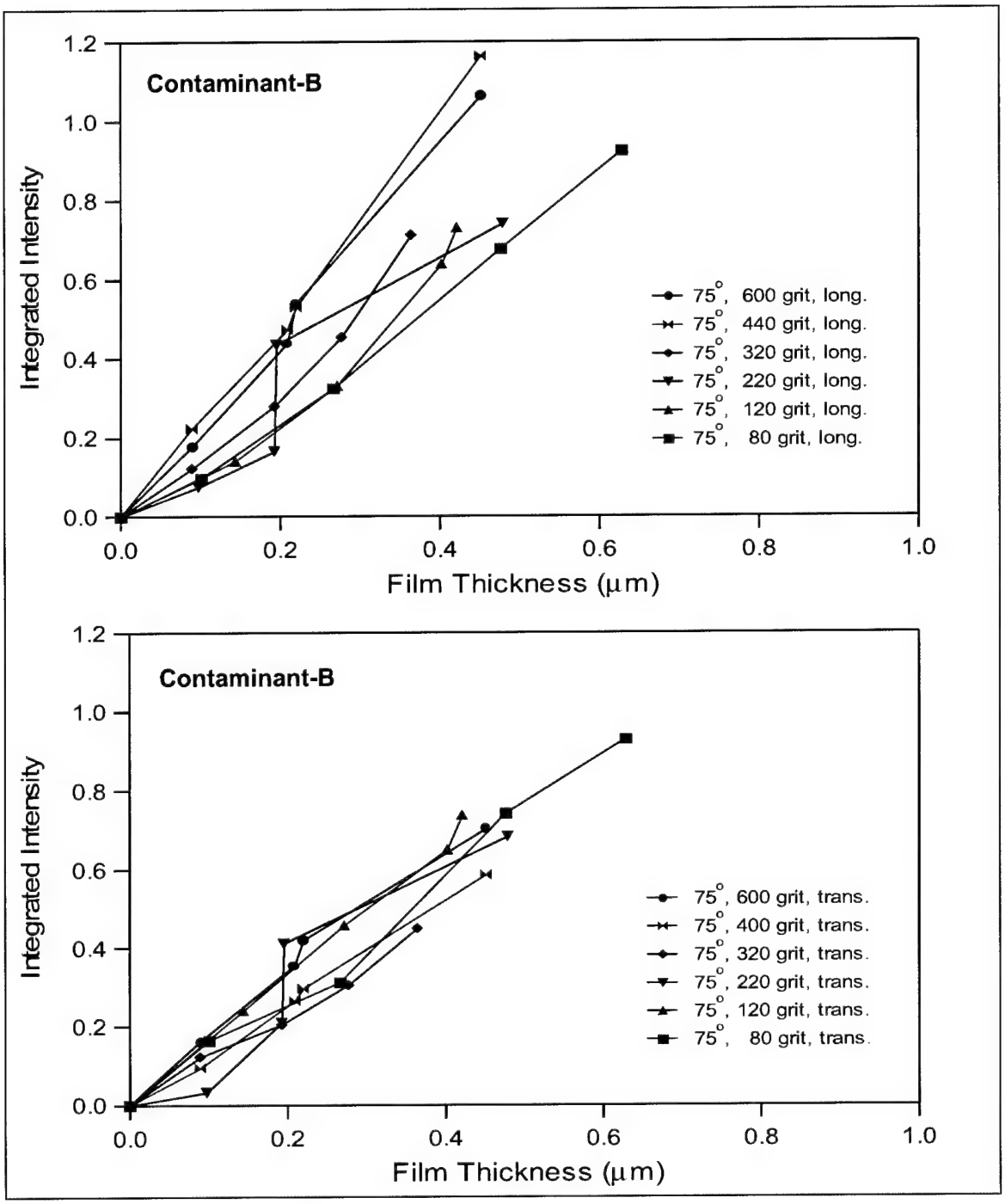

Figure 27. Integrated C-H peak intensity for spectrum of Contaminant B on aluminum.

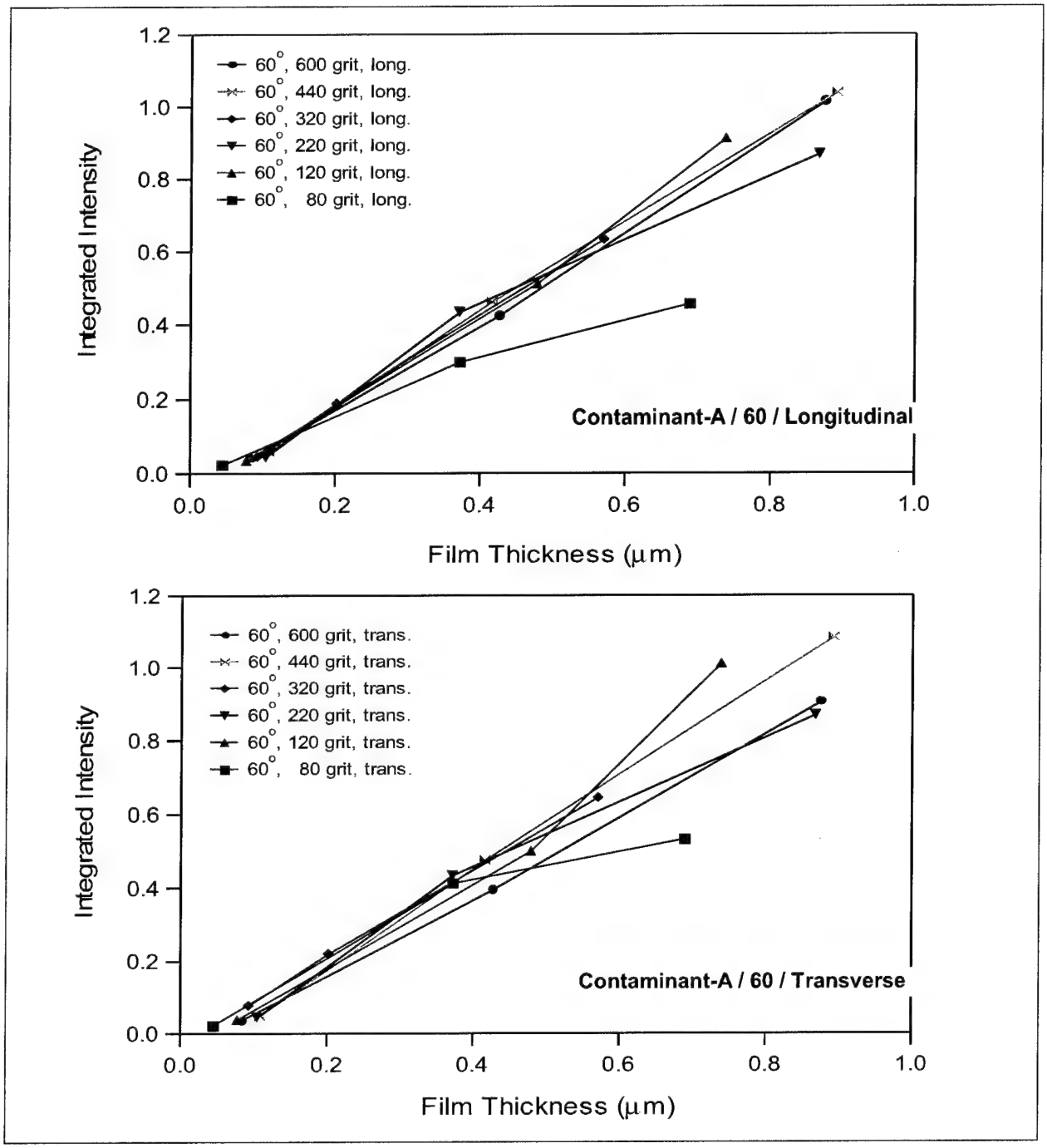

Figure 28. Integrated C-H peak intensities for spectrum of Contaminant A on aluminum at 60°.

Area integration calculations were performed by NFESC on longitudinally oriented aluminum panels soiled with contaminant C (Figure 29). There is a slight downward curvature at the highest film thickness value for the smoothest panel. Unexpectedly, the 400 and 320 grit data curve more severely than the rougher panel data. The 80 grit (roughest) data have a slight upward curvature. These inconsistencies may be caused by the difficulty of film application for contaminant C. The panels were each sampled at only one location on the contaminated surface. Uneven film application would cause non-linear peak integration values, depending on the exact surface location chosen for the analysis. Additionally, the profilometer data reveal that R_a differences for longitudinal orientation are not as extreme as the differences for transverse orientation.

The difference in spectral intensity for 60 degrees versus 75 degrees is displayed in Figure 30. The 75-degree data are decidedly more intense. The 60-degree data appear to be slightly more linear for the smoothest sample. The 60-degree data for contaminant A were obtained on Sandia National Laboratories' reflective sampling device. Corresponding contaminant C data were obtained from NFESC's selected optical interface.

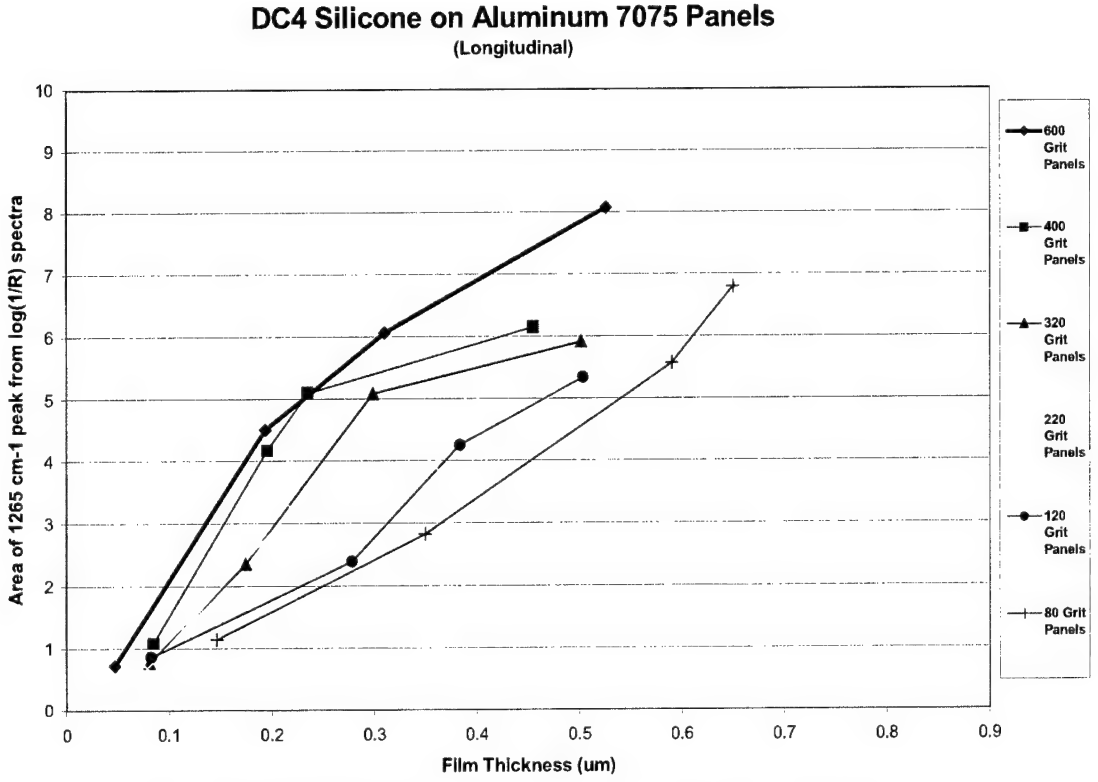

Figure 29. Comparison of spectral response linearity for surface roughness values 600 to 80 grit.

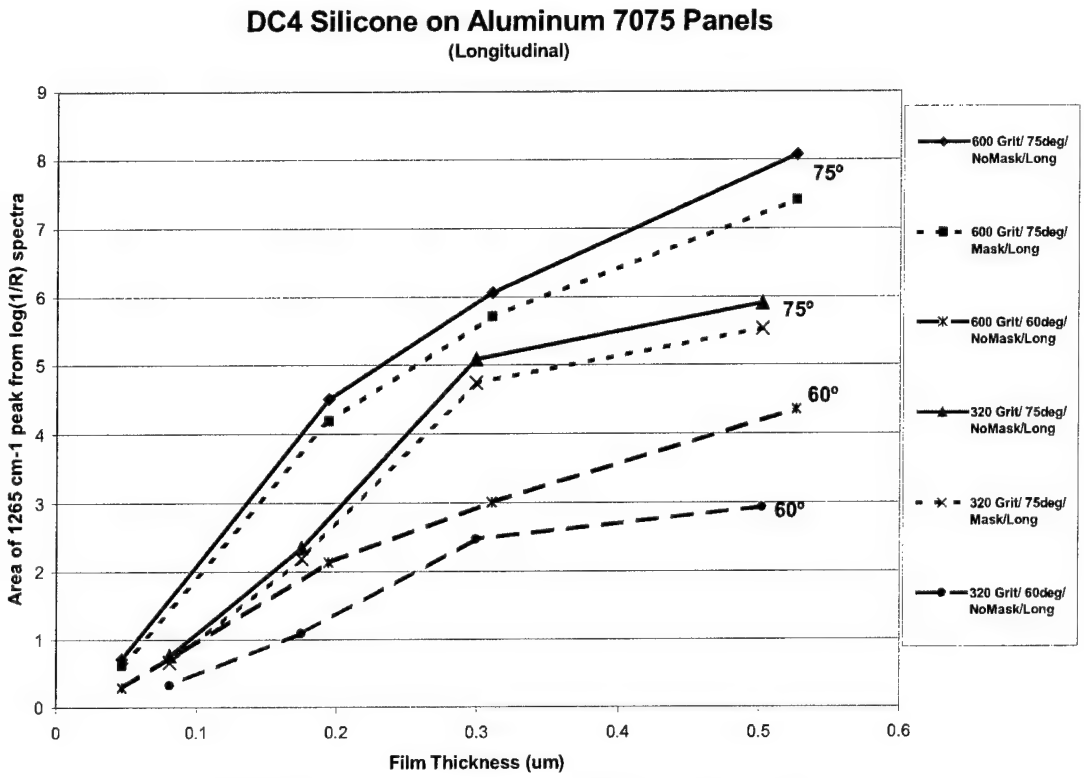

Figure 30. Comparison of spectral intensity for Contaminant-C at 60° and 75°.

4.2.4. Water vapor results

Applications of the real-time grazing-angle reflectance device will include environments where water-based cleaning processes are used. Water strongly absorbs radiation in two regions of the infrared spectrum, complicating the FTIR spectra. These absorption peaks may obliterate contaminant peaks falling in the same spectral region, or may distort the overall shape of the spectrum.

Results of the residual water interference experiment, described in the Section 3.3.4, are presented in Figure 31. The spectra reflect varying levels of water on the surface of an aluminum test coupon soiled with approximately 0.2 μm of contaminant B. The regions with pronounced spiking represent water vapor. The lower wavenumber region of the spectrum is obscured by the absorption peaks of the thickest water film. However, the C-H stretching peaks at 3,200 to 2,800 cm^{-1} are plainly visible with no interference of the baseline by the water absorption above 3,000 cm^{-1}. For a hydrocarbon contaminant such as B, an analyst could easily classify the material as a paraffin or aromatic hydrocarbon, but further identification (other molecular functional groups) would depend on the film thickness of the water residue. A water film of less than approximately 5 μm would still allow identification of functional groups for a contaminant film of greater than 0.1 μm.

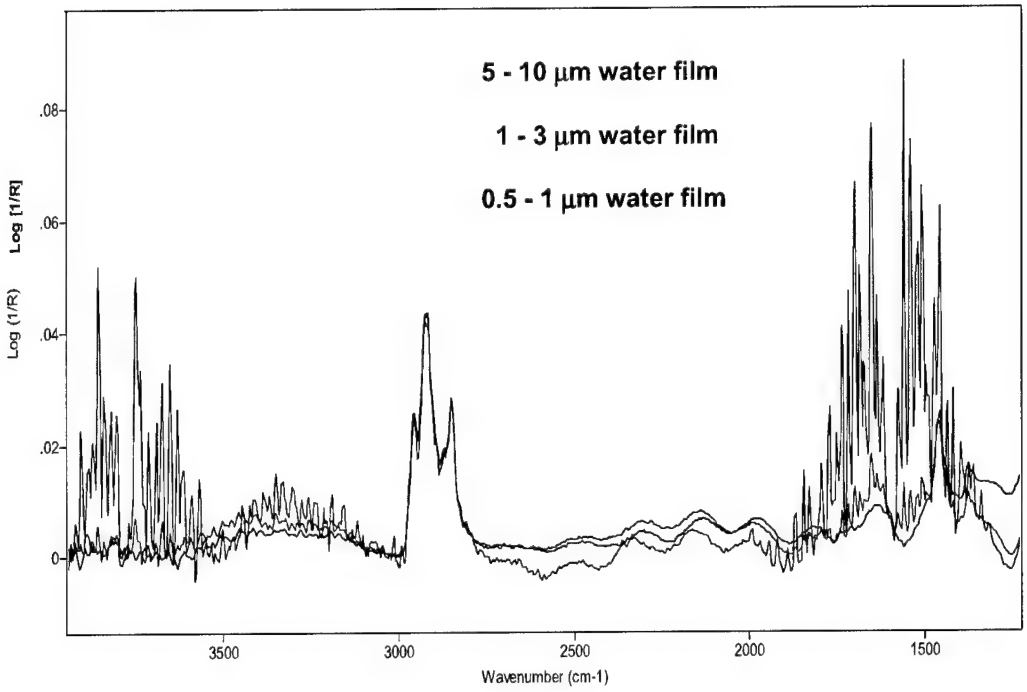

Figure 31. Water on aluminum panel previously soiled with 0.22 μm contamination B.

4.2.5. Curved reflective surfaces

Spectra of four of the six aluminum cylinders analyzed are presented in Figure 32. At every film thickness, the spectrum shows clearly defined C-H stretching peaks with relatively little noise in the baseline. Functional group absorbance at the lower wavenumbers is well-defined for the contaminant films above 0.2 μm in thickness. It is evident that the FTIR grazing angle method is capable of producing readable spectra for very thin films on curved, smooth-reflective surfaces down to 1-cm radius of curvature.

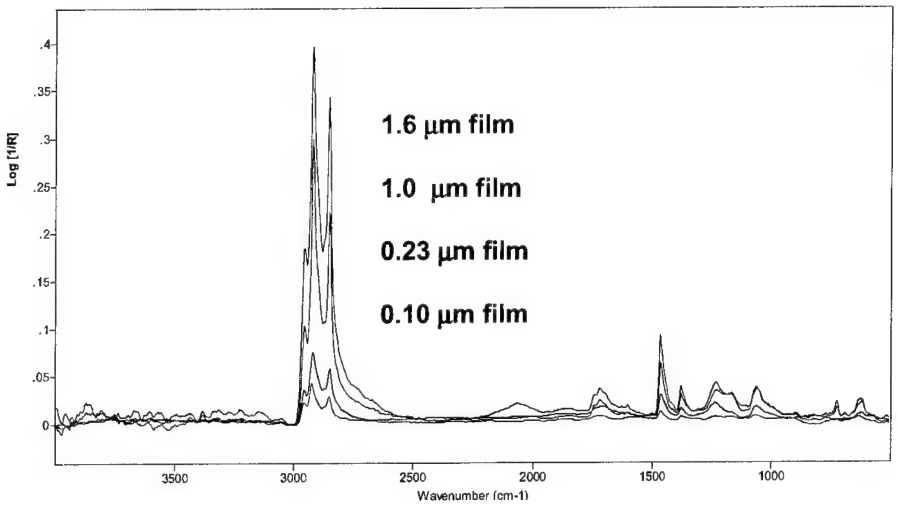

Figure 32. Contaminant B on aluminum cylinders (1-cm radius) at 75° and longitudinal orientation.

The effect of orienting the samples with their cylindrical axis both longitudinal and transverse to the infrared beam is shown in Figure 33 for the 0.2-µm film sample. As expected, reflectance spectra acquired at 75 degrees angle of incidence show an enhancement of absorption intensity relative to those at 60 degrees. We also observe, however, that the absorption intensities are also significantly greater for the transverse sample orientations at both angles of incidence. This trend is the opposite behavior observed for flat test coupons above.

Due to the very smooth surface of these aluminum substrates, enhancement of absorption spectra due to sample roughness as a function of orientation is not an important factor for these measurements. We believe that a more important aspect of the reflection-absorption intensity is its critical dependence on sample alignment with the optical interface collection optics. The observed behavior in these measurements may represent the relative difficulty in collecting longitudinally reflected from the highly curved surfaces. Although the initial results for these samples are encouraging, additional work is necessary to quantify and control the effects of sample orientation.

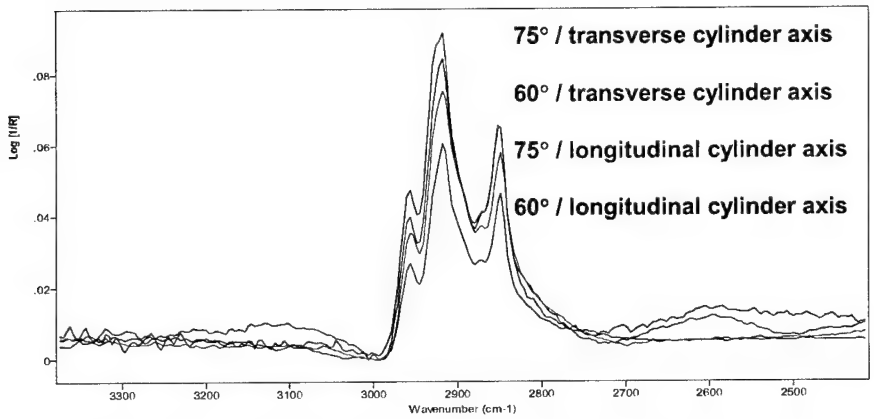

Figure 33. 0.2 μm contaminant B on aluminum cylinder at 75° and 60° and at both orientations.

5. DISCUSSION AND CONCLUSIONS

During Year 1 of the project, the feasibility of grazing-angle reflectance FTIR was successfully demonstrated for the detection of contaminant residues common to DOD components. The performance of the technique was evaluated as a function of contaminant species, film thickness, substrate reflectivity, surface roughness, presence of water interference, and sample curvature.

The three contaminants selected for the study are all used in DOD fabrication or repair facilities (applications given in Table 1) and are known for their resistance to removal during cleaning operations. The varying solubility and opacity of the materials served to reveal the linear range of the grazing-angle method for organic materials with these properties.

Determining the linear range of instrument response is necessary for quantification of film thickness. In a shop environment, knowing the film thickness of the contaminant on a component's surface allows the analyst to make decisions to implement or change a cleaning process. A process that over-cleans its parts is a waste of resources, time, and money. A process that under-cleans may result in a costly and subsequent serious part or assembly failure. Depending on the part's function, required cleanliness levels will vary. Sub-micrometer detection, for example, would be essential for determining low levels of silicones on aircraft parts. New mandatory low volatile organic content (VOC) coatings used on aircraft skins are very sensitive to silicone contaminants. These contaminants are known to leach out of door and window seals. The low levels would not be visible to the naked eye but may still require removal to prevent disbonding of the coating.

The test samples prepared for this study were of known surface areas and weight, and the specific gravity of the oven-dried contaminants was determined. These parameters were used to determine contaminant film thickness. These samples, then,

serve as calibration standards for like-parts containing unknown amounts of the material. Similar standards would be prepared for real-time operations.

Three more unique materials have been identified as common contaminants in DOD facilities. These include a hydraulic fluid, a rosin flux material, and a mold-release agent. These materials will be examined during Year 2 of the project.

Inorganic surface contaminants, such as rust or scale, were not evaluated at this time. The FTIR technique is capable of detecting a number of metal oxides, but analysis is complicated by the lack of available data on the optical properties of these materials. These optical property values are needed to perform theoretical calibrations of film thickness and composition, since preparation of actual thin film standards would be extremely difficult due to a lack of solubility for these materials.

Sandia National Laboratories has produced computer codes to generate optical constant values for a variety of materials on metal substrates (Ref. 11). NFESC has been working with Sandia National Laboratories to generate optical constants and subsequent theoretical or "calculated" spectra for the organic contaminants used in this study. The theoretical spectra serve to verify and predict the film thickness values obtained from weighed contaminants. Preliminary results indicate a lack of agreement between the theoretical and experimental spectral intensities. Potential causes include the particular design of NFESC's laboratory optical interface (lack of spectral linearity for the thicker films), and inadequate reference optical constants for real surfaces. These issues will be addressed in Year 2 of the project.

The variety of substrate materials evaluated in this study reflects many of the metals actually used in assemblies of DOD aircraft, weapons, and other components. NFESC successfully demonstrated the grazing-angle technique's ability to provide readable infrared spectra for these materials.

The reflectivity of non-metals varies widely. Non-metallic substrates that contain organic content will absorb infrared radiation and these absorptions are mixed into the resulting spectrum of the contaminant film. This reduces the overall energy that reaches the FTIR detector and complicates interpretation of the spectra. The p-component of incident radiation is not as greatly enhanced for non-metals as with metals (Ref. 12). Also, the optimal angle of incidence varies with the substrate type for non-metals and may even be below 60 degrees, the grazing angle threshold. Non-metallic composite materials are used in a variety of DOD components (e.g., in aircraft wings). In Year 2, at least one representative composite substrate will be evaluated for its ability to reflect infrared light without interfering with thin films on its surface.

Effects of surface roughness were thoroughly evaluated for reflective surfaces with profiles of approximately 0.30 to 6.0 μm (11 to 240 μin). In general, there was noticeable degradation in the overall quality of the spectra for films less than 0.2 μm at 320 and lower grit sizes. This manifested itself in baseline degradation as increased noise and increased fringe patterns, causing obscuration of peaks. This is especially evident at higher wavenumbers. C-H stretching peaks, however, in the 3,000 to 2,800 cm^{-1} range were often still visible upon expansion of the spectrum, allowing the analyst to classify the types of C-H functional groups present in the contaminant.

Interference from surface water residue was evaluated at varying levels of water thickness. IR absorbance by the water did not interfere with the CH stretching peaks in the upper region of the spectrum even at 5 to 10 μm (water visible to the naked eye),

but did obscure contaminant peaks in the lower region of the spectrum. Based on the observed evaporation rates of the water during this study, it is anticipated that water on the surfaces of shop parts in real-world cleaning operations will not significantly impair the FTIR method. Large amounts of water will need to be removed from the parts by hanging, rotation, shaking, or other appropriate means. The leftover water is expected to be $\leq$ 10 to 20 μm and to evaporate below the 5 to 10 μm level within 1 to 2 minutes in an ambient atmosphere. Studies during Year 2 will include the analysis of actual parts from military cleaning facilities. Water absorption by and reaction with various contaminants will be evaluated for their effect on the FTIR spectra.

Curved reflective surfaces were studied using 1-cm radius aluminum cylinders contaminated with Contaminant B. Excellent signal-to-noise levels were observed for both longitudinal and transverse analyses. This indicates that reflective surfaces of at least 1-cm convex radius of curvature are amenable to the grazing-angle technique.

Concave curvatures were not evaluated during Year 1. These surfaces present a much greater challenge for the grazing-angle technique. Unless the illuminated spot (typically 10 to 12 mm in diameter) is flat and the hollowed area wide and shallow, irradiating a concave surface will result in the reflected beam going astray and causing significant alteration of the reflected angle. The attenuated beam may not even reach the collection optics, which are aligned for grazing angle reflection. Additionally, the geometry of the sample may cause physical blockage of incident and reflecting light. Figure 34 illustrates this problem. On the convex side of the sample, the beam has no difficulty in reaching the surface. For the concave side, the edges of the hollowed region are impeding the path of the beam. Also, the reflected light has a shallower angle because of the inward curvature at the point of reflection. During Year 2 of the project, a threshold concave radius of curvature will be determined using real-world parts and the portable FTIR prototype. It is expected that this value will be much larger than the convex value demonstrated in Year 1.

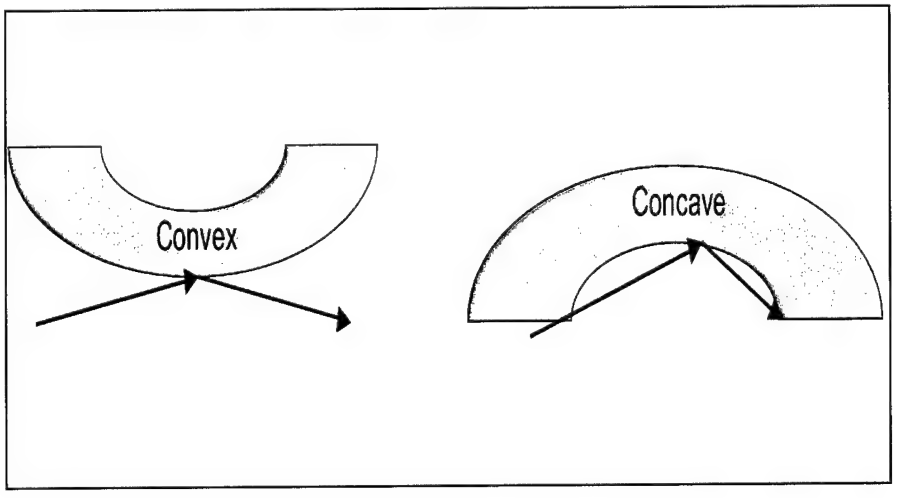

Figure 34. Infrared beam reflecting off of convex and concave surfaces

In summary, the following conclusions were established during Year 1 of the SERDP Online Surface Cleanliness Project.

a. Grazing-angle reflectance FTIR is a viable method for parts cleanliness analysis for reflective surfaces and organic contaminants. Excellent sensitivity to organic compounds is observed at 75-degree angle of incidence.
b. Signal-to-noise levels for both flat and cylindrical samples are adequate to allow for detection of very thin films (< 0.1 μm for flat).
c. Linear quantitative response is achieved for films ≤ 0.5 μm, or higher depending on type of contaminant and substrate.
d. The amount of infrared scattering and the quality of FTIR spectra are affected by surface roughness. However readable spectra are obtainable for very thin films even at R_a values of 6 μm.
e. Water residue over the surface of the contaminant begins to interfere with spectral interpretation at approximately 5 μm for flat samples.

Issues and recommendations for Year 2:

a. The grazing angle method is not well-suited for organic substrates (non reflective, non-metal). Investigate limitations using a DOD facility composite material.
b. Continue baseline measurements in the laboratory on calibrated contaminant samples.
c. Design and build the portable grazing-angle reflectance device.
d. The method requires calibrated samples for quantitative analyses. Investigate options to build calibration curves for the portable device.
e. Collect and analyze DOD hardware samples (including non-flat surfaces) for both the laboratory and portable devices.

6. ACKNOWLEDGEMENTS

This work was sponsored by the U.S. Department of Defense Strategic Environmental Research and Development Program (SERDP). The authors gratefully acknowledge Dr. David Ottesen, Dr. Peter Ludowise, and Mr. Howard Johnsen of Sandia National Laboratories for providing integration graphics and the noise-level calculations.

7. REFERENCES

1. Francis, S.A., and Ellison, A.H., J. Opt Soc. Am., 49, 131, 1959.
2. Greenler, R.G.J., "Infrared Study of Adsorbed Molecules on Metal Surfaces by Reflection Techniques." J. Chem. Phys., 44(1), 310-15, 1966.
3. Smith, B.C., Fundamentals of Fourier Transform Infrared Spectroscopy, CRC Press LLC, 1996.
4. Ulman, A., Ed. Characterization of Organic Thin Films, Materials Characterization Series, Butterworth-Heinemann, Stoneham MA, 1995.
5. Ferraro, J.R. and Basile, L.J., Ed. Fourier Transform Infrared Spectroscopy – Applications to Chemical Systems, Vol. 4, Academic Press, Inc., New York, 1985.
6. "External Reflectance Spectroscopy of Surfaces," Spectra-Tech FT-IR Technical Note TN-3, SpectaTech, Inc., 1998.
7. Ottesen, D., et al., "Cleaning Verification Monitor Technique Based on Infrared Optical Methods," FY1999 Annual Report, Strategic Environmental Research and Development Program, Project PP-1138, December 1999.
8. Kodres, C.A. et al., "Surface Quality Impact of Replacing Vapor Degreasers With Aqueous Immersion Systems," Naval Facilities Engineering Service Center Technical Report, NFESC TR-2067-ENV, 1997.
9. Ludowise, P., Ottesen, D., et al., "A PPLN laser-based system for chemical imaging," SPIE Conference On Imaging Spectrometry V, Denver CO, July 1999.
10. Technical specifications for the optical interface and the FTIR instrument, obtained from Pike Technologies and Biorad Corporation, respectively, 1999.
11. Ottesen, D.K., et al., "The Detection of Contaminants in Narrow-Bore tubing by Infrared Reflection Spectroscopy," Sandia National Laboratories Report SAND86-8789, Reprint, 1992.
12. Griffiths, P.R. and de Haseth, J.A., Fourier Transform Infrared Spectrometry, Chemical Analysis Vol. 83, John Wiley & Sons, New York, 1986.

APPENDIX A

Matrix of Calibrated Samples for Laboratory Grazing-angle reflectance FTIR Demonstration

Year 1

Sample ID	Geometry	Substrate	Contaminant	[illegible]	Residue Weight	Estimated Film Thickness*
416	1.5" x 5" flat panel	Aluminum 7075-T6	A	600 grit	0.00038	0.0847 um
415	1.5" x 5" flat panel	Aluminum 7075-T6	A	600 grit	0.00192	0.4280 um
413	1.5" x 5" flat panel	Aluminum 7075-T6	A	600 grit	0.00393	0.8762 um
336	1.5" x 5" flat panel	Aluminum 7075-T6	A	400 grit	0.00049	0.1092 um
334	1.5" x 5" flat panel	Aluminum 7075-T6	A	400 grit	0.00187	0.4169 um
331	1.5" x 5" flat panel	Aluminum 7075-T6	A	400 grit	0.00400	0.8918
257	1.5" x 5" flat panel	Aluminum 7075-T6	A	320 grit	0.00042	0.0936
254	1.5" x 5" flat panel	Aluminum 7075-T6	A	320 grit	0.00091	0.2029
255	1.5" x 5" flat panel	Aluminum 7075-T6	A	320 grit	0.00256	0.5707
006	1.5" x 5" flat panel	Aluminum 7075-T6	A	220 grit	0.00047	0.1048
004	1.5" x 5" flat panel	Aluminum 7075-T6	A	220 grit	0.00167	0.3723
001	1.5" x 5" flat panel	Aluminum 7075-T6	A	220 grit	0.00389	0.8672
106	1.5" x 5" flat panel	Aluminum 7075-T6	A	120 grit	0.00035	0.0780
105	1.5" x 5" flat panel	Aluminum 7075-T6	A	120 grit	0.00215	0.4793
104	1.5" x 5" flat panel	Aluminum 7075-T6	A	120 grit	0.00331	0.7379
206	1.5" x 5" flat panel	Aluminum 7075-T6	A	80 grit	0.00020	0.0446
204	1.5" x 5" flat panel	Aluminum 7075-T6	A	80 grit	0.00167	0.3723

Sample ID	Geometry	Substrate	Contaminant			Estimated Film Thickness*
201	1.5" x 5" flat panel	Aluminum 7075-T6	A	80 grit	0.00309	0.6889
418	1.5" x 5" flat panel	Aluminum 7075-T6	B	600 grit	0.00033	0.0897
420	1.5" x 5" flat panel	Aluminum 7075-T6	B	600 grit	0.00077	0.2093
419	1.5" x 5" flat panel	Aluminum 7075-T6	B	600 grit	0.00081	0.2203
417	1.5" x 5" flat panel	Aluminum 7075-T6	B	600 grit	0.00166	0.4514
338	1.5" x 5" flat panel	Aluminum 7075-T6	B	400 grit	0.00038	0.1033
339	1.5" x 5" flat panel	Aluminum 7075-T6	B	400 grit	0.00073	0.1985
340	1.5" x 5" flat panel	Aluminum 7075-T6	B	400 grit	0.00097	0.2638
337	1.5" x 5" flat panel	Aluminum 7075-T6	B	400 grit	0.00182	0.4949
259	1.5" x 5" flat panel	Aluminum 7075-T6	B	320 grit	0.00033	0.0897
261	1.5" x 5" flat panel	Aluminum 7075-T6	B	320 grit	0.00071	0.1931
260	1.5" x 5" flat panel	Aluminum 7075-T6	B	320 grit	0.00102	0.2774
258	1.5" x 5" flat panel	Aluminum 7075-T6	B	320 grit	0.00134	0.3644
008	1.5" x 5" flat panel	Aluminum 7075-T6	B	220 grit	0.00036	0.0979
009	1.5" x 5" flat panel	Aluminum 7075-T6	B	220 grit	0.00071	0.1930
010	1.5" x 5" flat panel	Aluminum 7075-T6	B	220 grit	0.00072	0.1958
007	1.5" x 5" flat panel	Aluminum 7075-T6	B	220 grit	0.00179	0.5167
108	1.5" x 5" flat panel	Aluminum 7075-T6	B	120 grit	0.00053	0.1441
109	1.5" x 5" flat panel	Aluminum 7075-T6	B	120 grit	0.00100	0.2719
110	1.5" x 5" flat panel	Aluminum 7075-T6	B	120 grit	0.00148	0.4025
107	1.5" x 5"	Aluminum 7075-T6	B	120 grit	0.00155	0.4215

Sample ID	Geometry	Substrate	Contaminant		Residue Weight	Estimated Film Thickness*
	flat panel					
208	1.5" x 5" flat panel	Aluminum 7075-T6	B	80 grit	0.00037	0.1006
209	1.5" x 5" flat panel	Aluminum 7075-T6	B	80 grit	0.00098	0.2665
210	1.5" x 5" flat panel	Aluminum 7075-T6	B	80 grit	0.00175	0.4759
207	1.5" x 5" flat panel	Aluminum 7075-T6	B	80 grit	0.00231	0.6282
004	1-cm radius cylinder	Aluminum Foil	B	Smooth	0.00039	0.106
005	1-cm radius cylinder	Aluminum Foil	B	Smooth	0.00055	0.150
003	1-cm radius cylinder	Aluminum Foil	B	Smooth	0.00072	0.196
001	1-cm radius cylinder	Aluminum Foil	B	Smooth	0.00084	0.228
002	1-cm radius cylinder	Aluminum Foil	B	Smooth	0.00371	1.009
006	1-cm radius cylinder	Aluminum Foil	B	Smooth	0.00541	1.471
422	1.5" x 5" flat panel	Aluminum 7075-T6	C	600 grit	0.00025	0.0470
423	1.5" x 5" flat panel	Aluminum 7075-T6	C	600 grit	0.00103	0.1935
421	1.5" x 5" flat panel	Aluminum 7075-T6	C	600 grit	0.00165	0.3100
424	1.5" x 5" flat panel	Aluminum 7075-T6	C	600 grit	0.00280	0.5261
342	1.5" x 5" flat panel	Aluminum 7075-T6	C	400 grit	0.00045	0.0845
343	1.5" x 5" flat panel	Aluminum 7075-T6	C	400 grit	0.00104	0.1954
341	1.5" x 5" flat panel	Aluminum 7075-T6	C	400 grit	0.00125	0.2348
344	1.5" x 5" flat panel	Aluminum 7075-T6	C	400 grit	0.00242	0.4547
264	1.5" x 5" flat panel	Aluminum 7075-T6	C	320 grit	0.00043	0.0808
265	1.5" x 5" flat panel	Aluminum 7075-T6	C	320 grit	0.00093	0.1747
263	1.5" x 5" flat panel	Aluminum 7075-T6	C	320 grit	0.00159	0.2987
266	1.5" x 5" flat panel	Aluminum 7075-T6	C	320 grit	0.00267	0.5016
012	1.5" x 5"	Aluminum 7075-T6	C	220 grit	0.00042	0.0789

Sample ID	Geometry	Substrate	Contaminant	[illegible]	Residue Weight	Estimated Film Thickness*
	flat panel					
013	1.5" x 5" flat panel	Aluminum 7075-T6	C	220 grit	0.00117	0.2198
001	1.5" x 5" flat panel	Aluminum 7075-T6	C	220 grit	0.00190	0.3570
014	1.5" x 5" flat panel	Aluminum 7075-T6	C	220 grit	0.00435	0.8173
112	1.5" x 5" flat panel	Aluminum 7075-T6	C	120 grit	0.00044	0.0827
113	1.5" x 5" flat panel	Aluminum 7075-T6	C	120 grit	0.00148	0.2781
111	1.5" x 5" flat panel	Aluminum 7075-T6	C	120 grit	0.00204	0.3833
114	1.5" x 5" flat panel	Aluminum 7075-T6	C	120 grit	0.00268	0.5035
212	1.5" x 5" flat panel	Aluminum 7075-T6	C	80 grit	0.00078	0.1465
213	1.5" x 5" flat panel	Aluminum 7075-T6	C	80 grit	0.00186	0.3495
211	1.5" x 5" flat panel	Aluminum 7075-T6	C	80 grit	0.00314	0.5899
214	1.5" x 5" flat panel	Aluminum 7075-T6	C	80 grit	0.00346	0.6501
Ti5-02	1.5" x 5" flat panel	Titanium 6Al-4V	C	600 grit	0.00040	0.0752
Ti5-03	1.5" x 5" flat panel	Titanium 6Al-4V	C	600 grit	0.00083	0.1559
Ti5-01	1.5" x 5" flat panel	Titanium 6Al-4V	C	600 grit	0.00230	0.4321
Ti5-04	1.5" x 5" flat panel	Titanium 6Al-4V	C	600 grit	0.00373	0.7008
Ti5-42	1.5" x 5" flat panel	Titanium 6Al-4V	C	220 grit	0.00066	0.1240
Ti5-43	1.5" x 5" flat panel	Titanium 6Al-4V	C	220 grit	0.00099	0.1860
Ti5-44	1.5" x 5" flat panel	Titanium 6Al-4V	C	220 grit	0.00222	0.4171
Ti5-41	1.5" x 5" flat panel	Titanium 6Al-4V	C	220 grit	0.00225	0.4227
304-42S	1.5" x 5" flat panel	Stainless Steel 304	C	600 grit	0.00068	0.1278
304-43S	1.5" x 5"	Stainless Steel 304	C	600 grit	0.00086	0.1616

Sample ID	Geometry	Substrate	Contaminant			Estimated Film Thickness*
	flat panel					
304-44S	1.5" x 5" flat panel	Stainless Steel 304	C	600 grit	0.00273	0.5129
304-41S	1.5" x 5" flat panel	Stainless Steel 304	C	600 grit	0.00276	0.5185
304-43R	1.5" x 5" flat panel	Stainless Steel 304	C	220 grit	0.00098	0.1841
304-42R	1.5" x 5" flat panel	Stainless Steel 304	C	220 grit	0.00104	0.1954
304-44R	1.5" x 5" flat panel	Stainless Steel 304	C	220 grit	0.00187	0.3513
304-41R	1.5" x 5" flat panel	Stainless Steel 304	C	220 grit	0.00289	0.5430
C4340-42S	1.5" x 5" flat panel	Stainless Steel 304	C	600 grit	0.00060	0.1127
C4340-43S	1.5" x 5" flat panel	Stainless Steel 304	C	600 grit	0.00146	0.2743
C4340-41S	1.5" x 5" flat panel	Stainless Steel 304	C	600 grit	0.00185	0.3476
C4340-44S	1.5" x 5" flat panel	Stainless Steel 304	C	600 grit	0.00215	0.4039
C4340-42R	1.5" x 5" flat panel	Stainless Steel 304	C	220 grit	0.00058	0.1090
C4340-43R	1.5" x 5" flat panel	Stainless Steel 304	C	220 grit	0.00072	0.1353
C4340-44R	1.5" x 5" flat panel	Stainless Steel 304	C	220 grit	0.00240	0.4509
C4340-41R	1.5" x 5" flat panel	Stainless Steel 304	C	220 grit	0.00285	0.5355

*Based on specific gravity of oven-dried sample of contaminant

A: 0.927 gm/cc

B: 0.76 gm/cc

C: 1.1 gm/cc